SIGNIFICANCE OF HALL CURRENT AND ION SLIP IN A THREE DIMENSIONAL MAXWELL NANOFLUID FLOW OVER ROTATING DISK WITH VARIABLE CHARACTERISTICS

STUDENT NAME: JAWAD ALI

ENROLLMENT NO: 01-248202-006

SUPERVISOR BY Prof. Dr. MUHAMMAD RAMZAN

A thesis submitted in fulfilment of the requirements for the award of degree of Masters of Science (Mathematics)

Department of Computer Science

BAHRIA UNIVERSITY ISLAMABAD

Session (2020-2022)

Approval of Examination

Scholar Name: Jawad ali

Registration Number: 71098

Enrollment: 01-248202-006

Program of Study: : MS (Mathematics)

Thesis Title: Significance of Hall current and Ion slip in a three dimensional Maxwell nanofluid flow over a rotating disk with variable characteristics.

It is to certify that the above scholar's thesis has been completed to my satisfaction and, to my belief, its standard is appropriate for submission for examination. I have also conducted plagiarism test of this thesis using HEC prescribed software and found similarity index 18% that is within the permissible limit set by the HEC for the MS/M. Phil degree thesis. I have also found the thesis in a format recognized by the BU for the MS/M. Phil thesis.

Supervisor Name: Prof. Dr. Muhammad Ramzan

Supervisor Signature:

Date:

Author's Declaration

I,JAWAD ALI hereby state that my MS/MPhil thesis titled " Significance of Hall current and Ion slip in a three dimensional Maxwell nanofluid flow over a rotating disk with variable characteristics " is my own work and has not been submitted previously by me for taking any degree from this university Bahria University or anywhere else in the country/world. At any time if my statement is found to be incorrect even after my Graduate the university has the right to withdraw/cancel my MS/MPhil degree

Name of Scholar:Jawad Ali

Date: 15/9/2022

Plagiarism Undertaking

I, solemnly declare that research work presented in the thesis titled" Significance of Hall current and Ion slip in a three dimensional Maxwell nanofluid flow over a rotating disk with variable characteristics " is solely my research work with no significant contribution from any other person. Small contribution / help wherever taken has been duly acknowledged and that complete thesis has been written by me.

I understand the zero tolerance policy of the HEC and Bahria University towards plagiarism. Therefore, I as an Author of the above titled thesis declare that no portion of my thesis has been plagiarized and any material used as reference is properly referred/ cited.

I undertake that if I am found guilty of any formal plagiarism in the above titled thesis even after award of MS/MPhil degree, the university reserves the right to withdraw / revoke my MS/MPhil degree and that HEC and the University has the right to publish my name on the HEC / University website on which names of students are placed who submitted plagiarized thesis.

Name of Scholar:jawad Ali

Date:15/09/2022

Dedication

My beloved parents, Habibullah and respected teachers.Thanks for your love, pray and support.

Acknowledgements

Praise to be Almighty Allah, who is the Lord of the world, the Answer of prayers and the source of peace, whose blessing and exaltation flourished to the scared wealth of knowledge. Indeed, this difficult task was made possible with the help of Allah. Special praise and regards for his Last messenger, Holy Prophet Hazrat Muhammad (PBUH). Holy Prophet said that I AM the light, whoever follows ME, will never be in the darkness.

I feel great pleasure in expressing my profound and heartiest gratitude to my kind, devoted supervisor Dr. Muhammad Ramzan for his indispensable guidance, deep consideration, affection and active co-operation that made possible to this work to meet its end successfully well in time. Teachers like him are very precious assets for a nation who change the life of an individual and also nations. Such teachers make the density of a nation. I am proud that my supervisor is also one of the teachers and working with him is an honor for me.

I would also express my gratitude to all teachers. Due to their guidance and help am able to get the success of reaching my destination. The prominent among them are Dr. Jafar Husnain and Dr. Rizwan ul Haq who supported me in all course work as well as in the completion of this thesis. I like to thanks to all respected teachers at Department of Mathematics, Bahria University Islamabad Campus for providing us healthy academic environment.

I express my gratitude to my family member who provided me every moral and financial during my study at Bahria University and thus I was able to accomplish core task of thesis, without their continuous help i could not imagine to achieve this goal. I am also thankful to my friends who provided me every assistance during my study, Hina Gul, Nazia Shahmir, Saima Riasat, and Naila Shaheen. At the end I would acknowledge the pleasant moments with my all fellows.

Abstract

This thesis discusses the three-dimensional Maxwell nanofluid flow over a rotating deformable disk influenced Hall current and Ion slip. To increase the stability of the nanofluid flow, the effect bio-convection are embedded. The novelty of thesis is enhanced by consideration of variable thermal conductivity and viscosity. The slip and convective condition are taken at the boundary of the surface. Von Karman similarity transformation are used to obtain the differential equations from partial equations. The problem is solved numerically by using the bvp4c technique of MAT-LAB software. To highlight the key effects of the problem, graphical illustrational are used. To authenticate the presented model a comparison is also made with a published work in limiting case. An excellent correlation is obtained here.

TABLE OF CONTENTS

.

LIST OF TABLES

LIST OF FIGURES

Nomenclature

Symbols

(u, v, w)	The velocity components in the direction of $(r, \theta, z)\left(ms^{-1}\right)$
f	Radial velocity profile
β	Casson fluid parameter
b	Rate of stretching
D_T	Thermophoretic diffusion coefficient, (m^2s^{-1})
D_B	Brownian diffusion coefficient
D_{B_∞}	Ambient diffusion coefficient (m^2s^{-1})
β_0	Magnetic field strength
p	pressure
h_2	Convective mass transfer coefficient
d_1	Variable thermal conductivity parameter
H_2	Biot number of mass transfer
H_1	Biot number of heat transfer
K_1	Thermal relaxation parameter
K_2	Concentration relaxation parameter
β_i	Ion-Slip parameter
β_1	Maxwell parameter

Pr	Prandtl number
N_b	Brownian motion parameter
T	Temperature
M	Magnetic parameter
ρ	Density $\left(kgm^3\right)$
μ	Dynamic viscosity (m^2s^{-1})
Le	Lewis number
T_∞	Ambient temperature (k)
Pe	Peclet number
τ_{zr}	Radial direction of Shear stress
T_w	The temperature at the surface of the disk (k)
w_e	Constant speed of cell swimming.
p	Stretching rate to angular frequency
e	Variable molecular diffusivity parameter
C_∞	Ambient concentration
τ	The capacity ratio or heat capacity of solid particles and nanofluid.
Fr	Forchheimer number
$k(T)$	Variable thermal conductivity $(w(mk)^{-1})$
C_w	Concentration near the disk's surface
h	Axial velocity profile
c_p	Specific heat
g	Tangential velocity profile
h_1	Convective heat transfer coefficient
L	Velocity slip parameter

β_e	Hall current parameter
S_c	Schmidt number
N_t	parameter of Thermophoretic
S	First-order velocity slip coefficient
ν	Kinematic viscosity $(\mathrm{m^2 s^{-1}})$
D_n	Microorganism's diffusivity,
τ_w	shear stress
λ^*	Variable viscosity
λ_1	Heat flux relaxation of time
λ_2	Mass flux relaxation of time
Q^*	The angular velocity of the heat source parameter
λ_0	Relaxation time parameter
λ_o	Relaxation time parameter of maxwell fluid
$\tau_{z\theta}$	tangential shear stress
Q_w	Heat flux
Q_m	Mass flux

Chapter 1

BASIC PRELIMINARIES AND LAWS

This chapter contains some elementary definitions, concepts and laws that are helpful in understanding the works in the third and fourth chapters.

1.1 Fluid

A material that deforms under the influence of shear stress on a continuous basis. As examples of fluids, consider mercury, paints, oil, oxygen, and blood.

1.1.1 Liquid

It's a kind of fluid with a fixed volume but no specific shape. For examples water, oil, and milk.

1.1.2 Gas

A gas is a fluid that has no specified volume or shape. For example hydrogen, oxygen, and nitrogen etc.

1.2   Fluid mechanics

A branch of mechanics that deals with fluid properties is called fluid mechanics. It can be divided into two sub categories.

1.2.1   Fluid dynamics

It studies the properties of liquids in state of motion.

1.2.2   Fluid statics

It studies the properties of liquids in stationary state.

1.3   Stress

A stress is a force exerted on an infinitesimal surface element per unit area. The unit of stress in SI system is Nm^{-2} or $kg/m.s^2$ and dimension is given as $\left[\frac{M}{LT^2}\right]$.

$$\tau_{ji} = \frac{F_i}{A_j} \ , \qquad i,j = x,y,z, \qquad (1.1)$$

where A_j and F_i are the components of area and force respectively.

1.3.1   Shear stress

Force per unit area occurring parallel to an infinitesimal surface element is characterised as shear stress.

1.3.2   Normal stress

Force per unit area occurring perpendicular to an infinitesimal surface element is characterised as nomal stress.

1.4   Strain

Strain is the dimensionless quantity which is used to measure the deformation of an object when a force is applied on it.

1.5 Flow

It is specified as a substance that continually deforms under the impacts of distinct form of forces. Flow is further divided into two major categorised as follows:

1.5.1 Laminar flow

When the fluid moves in regular patterns with no overlapping of fluid layers is called laminar flow.

1.5.2 Turbulent flow

When the fluid moves in irregular patterns with overlapping of fluid layers layers is called Turbulent flow.

1.6 Viscosity

Viscosity is a basic component of fluids that determines the resistant to flow when multiple forces are acting on them. The viscosity can be described in two ways.

1.6.1 Dynamic viscosity (μ)

The maesure of internal resistance to flow is dynamic viscosity (μ), typically is termed as absolute viscosity. The following is the mathematical representation.

$$\text{viscosity } (\mu) = \frac{\text{shear stress } (\tau_{yx})}{\text{gradient of velocity}(\frac{\partial u}{\partial y})}. \tag{1.2}$$

Its unit is Kg/ms and its dimension is $ML^{-1}T^{-1}$.

1.6.2 Kinematic viscosity (ν)

The ratio of absolute viscosity (μ) to fluid density (ρ) is termed as kinematic viscosity. Mathematically it is represented by

$$\text{Kinematic viscosity}(\nu) = \frac{\text{Dynamic viscosity}}{\text{Fluid density}} = \frac{\mu}{\rho}. \tag{1.3}$$

Its dimensionis $\left[\frac{L^2}{T}\right]$ and its SI unit is $\frac{M^2}{T}$.

1.7 Newton's law of viscosity

Liquids which show the direct and linear corrpondence between velocity gradient and shear stress. Mathematically, it can be represented as follows:

$$\tau_{yx} \propto \frac{du}{dy}, \tag{1.4}$$

or

$$\tau_{yx} = \mu \left(\frac{du}{dy}\right). \tag{1.5}$$

In which τ_{yx} indicate the shear force applied on the fluid element and μ indicate the proportionality constant and $\left(\frac{du}{dy}\right)$ denotes the velocity gradient.

1.7.1 Non-Newtonian fluids

Fluids that doesnot satisfy the Newton law of viscosity and have a diifferent viscosity. Here, nonlinear and direct relationship exists between rate of shear deformation $\left(\frac{du}{dy}\right)$ and shear stress $(\boldsymbol{\tau}_{yx})$. Non-Newtonian fuids include toothpaste, butter, fabric paint etc. Mathematically it is expressed as.

$$\boldsymbol{\tau}_{yx} \propto \left(\frac{du}{dy}\right)^n, \ n \neq 1, \tag{1.6}$$

or

$$\boldsymbol{\tau}_{yx} = \eta_1 \frac{du}{dy}, \ \eta_1 = m \left(\frac{du}{dy}\right)^{n-1}, \tag{1.7}$$

where n the flow behaviour index, m the consistency index and η_1 the apparent viscosity. For $n = 1$ Eq. (2:7) converts to Newton's law of viscosity. Yougurt, fabric paints and ketchup exhibits the non-Newtonian fluid behavior. These fluids are divided into three types (i) differential type (ii) rate type (iii) integral type.

1.7.2   Newtonian fluids

The fluids that obey Newton law of viscosity and have a constant viscosity. In these fluids shear force (τ_{yx}) is proportional (linearly) to rate of shear deformation $\left(\frac{du}{dy}\right)$. Newtonian fluids include water, glycerol, alcohol, air, and thin motor oil throughout a wide range of shear rates and shear stresses seen in everyday life.
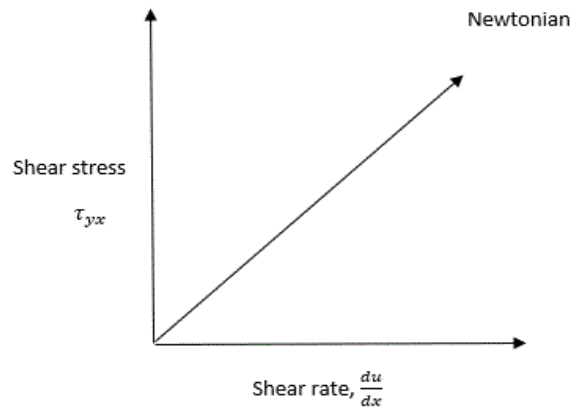
Fig. 1.1

1.8   Density

Mass of a material per unit volume is known as density. This quantity is used to measure the amount of matter that is present in a certain volume of it.

Mathematically expessed as follows:

$$\rho = \frac{m}{V}. \tag{1.8}$$

The SI unit of density is kg/m^3.

1.9　Pressure

Pressure is expressed as a magnitude of force applied perpendicular to the surface per unit area. Numerically, it is repsented as :

$$p = \frac{F}{A}. \tag{1.9}$$

Here, p is a pressure, F denotes force and A is the area of the surface. It's SI unit is Nm^{-2}.

1.9.1　Compressible fluid

The fluid having variable density is called as compressible fluid. Density and viscosity of a liquid increases with enhanced of pressure. For example mercury, gas, etc.

1.9.2　Incompressible fluid

The liquid having constant density is called Incompressible fluid. the variation of density in fluid flow with pressure increase or decrease is not high and it can be neglected. For example blood, air flow through a fan, etc.

1.10　Heat

Heat is the flow of energy from a warm object to a cold object.

1.11　Mechanism of heat transfer

Heat is a type of energy that moves from a hotter to a colder place. Heat transfer occurs when two materials of different temperatures come into contact with each other. Heat is dispersed by three basic mechanisms: conduction, radiation, and convection.

1.11.1　Conduction

Conduction is the process by which heat is transferred from a hot region to a cold region of solids and fluids through collisions of molecules and free electrons. Molecules are not transported in this reaction.

Mathematically

$$\frac{\mathbf{q}}{A} = k\left(\frac{T_1 - T_2}{X_1 - X_2}\right) = k\frac{\Delta T}{\Delta X}, \tag{1.10}$$

or

$$\mathbf{q} = -kA\frac{dT}{dx}, \tag{1.11}$$

where A the area of the surface, $\mathbf{q}$ represents the heat flow, k the thermal conductivity, T_2 temperature is less than T_1, The temperature gradient is denoted by $\frac{dT}{dx}$, and the negative sign implies that heat is transported from high to low temperature.

1.11.2 Convection

Convection occurs when a heated fluid, like as air or water, is pushed to move away from the source of heat, bringing energy with it.

Mathematically

$$\mathbf{q} = hA\left(T_s - T_\infty\right). \tag{1.12}$$

Here A for the area, T_∞ for the reference temperature, h is coefficient convective heat transfer , and T_s for the system temperature.

1.11.3 Radiation

A process in which the heat is transferred by the electromagetic waves is called radiation. This process plays vital role when heat is transferred through vacuum.

Mathematically

$$\mathbf{q} = e\sigma A\left(\Delta T\right)^4, \tag{1.13}$$

where e for emissivity of the system, $\mathbf{q}$ denotes the heat transfer, A for area, σ for the constant Stephen-Boltzmann, and $(\Delta T)^4$ for the temperature difference between two systems fourth power.

1.12   Slip boundary condition

The slip boundary condition, also known as the velocity-offset boundary condition, discontinuity in the velocity function, emplying that there is a relative motion between the fluid and the boundary. The hypothetical distance within the boundary at which the velocities functions would effectively influence the velocity of the boundary is referred to as slip length L. The difference between the velocity of the final layer of the fluid field and the velocity at the boundary may be approximated.

Mathematically

$$u - U_w = L\frac{\partial u}{\partial m}. \tag{1.14}$$

Here m is the perpendicular coordinate to thewall, L slip length, and $\frac{\partial u}{\partial z}$ slip velocity.

1.13   Convective boundary conditions

Convective boundary conditions are also known as Robin boundary conditions. This type of circumstance is frequently defned on a wall. These are stated mathematically as:

$$k\left(\frac{\partial T}{\partial m_i}\right)_{x_i} = h_f\left[T_f(x_i, t) - T_w(x_i, t)\right]. \tag{1.15}$$

This equation states that condition equals convection. Here x_i is the coordinate at the boundary, h_f indicates the heat transfer coefficient , T_w the wall temperature and T_f the fluid temperature.

1.14   Nanofluid

A nanofluid is a fluid that contains nano size nanoparticles with diameter less than 100 nanometers. The nanoparticles are usually made of carbon nanotubes, oxides, metals or carbides. Base fluid includes water, ethylene glycol and oil.

1.15 Casson fluid

The Casson fluid represents the shear thinning behaviour caused by yield stress. Fluid behaviour as a solid when shear stresses are applied that are less than the yield stress, but larger shear stresses cause it to deform. The Casson fluid model extra stress tensor is given as:

$$\tau_{ij} = \left(\mu_B + \frac{S_y}{\sqrt{2.\pi}}\right) 2\gamma_{ij}^*, \qquad if \quad \pi > \pi_c \ , \tag{1.16}$$

$$\tau_{ij} = \left(\mu_B + \frac{S_y}{\sqrt{2.\pi_c}}\right) 2\gamma_{ij}^*, \qquad if \quad \pi < \pi_c, \tag{1.17}$$

where $\pi = e_{ij}\gamma_{ij}^*$ and e_{ij} is the $(i,j)^{th}$ component of the deformation rate, μ_B is the dynamic viscosity of the non-Newtonian fluid, π_c is a critical value of this product based on the non-Newtonian model, S_y is the fluid stress, π is the product of the component of deformation rate with itself.

1.16 Maxwell fluid model

Maxwell liquid extra stress tensor is writen as:

$$\rho\left(\nabla.V\right).V = -\nabla.\rho + \nabla.E^\circ + J \times B, \tag{1.18}$$

$$J = \sigma\left(V \times B\right), \qquad B = [0, 0, B_O]. \tag{1.19}$$

Extra stress tensor E° for Maxwell liquid is

$$\left(1 + \lambda_o \frac{D}{Dt}\right) E^\circ = E^\circ + \lambda_o \frac{DE^\circ}{Dt} = \mu A_1, \tag{1.20}$$

where μ is the dynamic viscosity, λ_o stands for time relaxation time, A_1 for first Rivlin-Erickson tensor and $\frac{D}{Dt}$ for the distinction of covariant variables. First Rivlin-Erickson tensor is

$$A_1 = \left(\operatorname{grad} V\right)^t + \operatorname{grad} V, \tag{1.21}$$

in which t exhibits marrix transpose. For the three dimension flow we have

$$A_1 = \begin{pmatrix} \frac{\partial u_r}{\partial r} & \frac{\partial u_\theta}{\partial r} & \frac{\partial u_z}{\partial r} \\ \frac{1}{r}\frac{\partial u_r}{\partial \theta} - \frac{u_\theta}{r} & \frac{1}{r}\frac{\partial u_\theta}{\partial \theta} + \frac{u_r}{r} & \frac{1}{r}\frac{\partial u_z}{\partial \theta} \\ \frac{\partial u_r}{\partial z} & \frac{\partial u_\theta}{\partial z} & \frac{\partial u_z}{\partial z} \end{pmatrix} + \begin{pmatrix} \frac{\partial u_r}{\partial r} & \frac{\partial u_\theta}{\partial r} & \frac{\partial u_z}{\partial r} \\ \frac{1}{r}\frac{\partial u_r}{\partial \theta} - \frac{u_\theta}{r} & \frac{1}{r}\frac{\partial u_\theta}{\partial \theta} + \frac{u_r}{r} & \frac{1}{r}\frac{\partial u_z}{\partial \theta} \\ \frac{\partial u_r}{\partial z} & \frac{\partial u_\theta}{\partial z} & \frac{\partial u_z}{\partial z} \end{pmatrix}^t, \qquad (1.22)$$

$$A_1 = \begin{bmatrix} 2\frac{\partial u_r}{\partial r} & \frac{\partial u_\theta}{\partial r} + \frac{1}{r}\frac{\partial u_r}{\partial \theta} - \frac{u_\theta}{r} & \frac{\partial u_z}{\partial r} + \frac{\partial u_r}{\partial z} \\ \frac{\partial u_\theta}{\partial r} + \frac{1}{r}\frac{\partial u_r}{\partial \theta} - \frac{u_\theta}{r} & 2\left(\frac{1}{r}\frac{\partial u_\theta}{\partial \theta} + \frac{u_r}{r}\right) & \frac{1}{r}\frac{\partial u_z}{\partial \theta} + \frac{\partial u_\theta}{\partial z} \\ \frac{\partial u_r}{\partial z} + \frac{\partial u_z}{\partial r} & \frac{\partial u_\theta}{\partial z} + \frac{1}{r}\frac{\partial u_z}{\partial \theta} & 2\frac{\partial u_z}{\partial z} \end{bmatrix}, \qquad (1.23)$$

for the tensor E° of rank two, vector b_o and scalar φ, we have

$$\frac{DE^\circ}{Dt} = \frac{\partial E^\circ}{\partial t} + (\nabla.V)\,E^\circ - E^\circ\,(\mathrm{grad}\,V)^t - (\mathrm{grad}\,(V)\,E^\circ), \qquad (1.24)$$

$$\frac{Db_o}{Dt} = \frac{\partial b_o}{\partial t} + ((\nabla.V)\,b_o - \mathrm{grad}\,V)\,b_o, \qquad (1.25)$$

$$\frac{D\varphi}{Dt} = \frac{\partial \varphi}{\partial t} + (\nabla.V)\,\varphi. \qquad (1.26)$$

Applying the opertor $1 + \lambda_0 \frac{D}{Dt}$ on law of momentum conservation from Eq.(2.71), we get the folloing expression in the absence of body force

$$\rho\left(1 + \lambda_0 \frac{D}{Dt}\right)\frac{\partial v}{\partial t} = -\left(1 + \lambda_o \frac{D}{Dt}\right)\nabla_p + \left(1 + \lambda_o \frac{D}{Dt}\right)(\nabla.E^\circ). \qquad (1.27)$$

By adopting the procedure

$$\frac{D}{Dt}(\nabla) = \nabla.\left(\frac{D}{Dt}\right), \qquad (1.28)$$

applying equestions (2.28) in equestion (2.27), we obtain

$$\rho\left(1 + \lambda_0 \frac{D}{Dt}\right)\frac{\partial v}{\partial t} = -\left(1 + \lambda_1 \frac{D}{Dt}\right)\nabla_p + \left(1 + \lambda_o \frac{D}{Dt}\right)(\nabla.E^\circ), \qquad (1.29)$$

applying equestion (2.28) in equestion (2.29), we obtain

$$\rho\left(1 + \lambda_1 \frac{D}{Dt}\right)\frac{\partial v}{\partial t} = -\left(1 + \lambda_o \frac{D}{Dt}\right)\nabla_p + \mu.(\nabla.A_1). \qquad (1.30)$$

13

The above equation assumes the following form in the absence of a pressure gradient:

$$\rho \left(1 + \lambda_o \frac{D}{Dt}\right) \frac{\partial v}{\partial t} = \mu. \left(\nabla . A_1\right). \tag{1.31}$$

Thus, above expession for steady Maxwell liquid flow is expressed by:

$$u_r \frac{\partial u_r}{\partial r} + \frac{u_\theta}{r} \frac{\partial u_r}{\partial \theta} - \frac{v^2}{r} + u_z \frac{\partial u_r}{\partial z} =$$
$$\nu \left(\frac{1}{\partial r} \left(\frac{1}{r} \frac{\partial}{\partial r} \left(r u_r\right)\right) + \frac{1}{r^2} \frac{\partial^2 u}{\partial \theta^2} - \frac{2}{r^2} \frac{\partial u}{\partial \theta} + \frac{\partial^2 u_r}{\partial z^2}\right) -$$
$$\lambda_0 \left(u^2 \frac{\partial^2 u}{\partial r^2} + w^2 \frac{\partial^2 u}{\partial z^2} + 2uw \frac{\partial^2 u}{\partial r \partial z} - \frac{2uv}{r} \frac{\partial v}{\partial r} - \frac{2vw}{r} \frac{\partial v}{\partial z} + \frac{uv^2}{r^2} + \frac{v^2}{r} \frac{\partial u}{\partial r}\right), \tag{1.32}$$

$$u_r \frac{\partial u_\theta}{\partial r} + \frac{u_\theta}{r} \frac{\partial u_\theta}{\partial \theta} - \frac{u_r u_\theta}{r} + u_z \frac{\partial u_\theta}{\partial z} =$$
$$\nu \left(\begin{array}{c} \frac{1}{\partial r} \left(\frac{1}{r} \frac{\partial}{\partial r} \left(r u_\theta\right)\right) + \\ \frac{1}{r^2} \frac{\partial^2 u_\theta}{\partial \theta^2} - \frac{2}{r^2} \frac{\partial u_r}{\partial \theta} + \frac{\partial^2 u_\theta}{\partial z^2} \end{array} \right)$$
$$-\lambda_0 \left(\begin{array}{c} u_r^2 \frac{\partial^2 u_\theta}{\partial r^2} + u_z^2 \frac{\partial^2 u_\theta}{\partial z^2} + 2u_r u_\theta \frac{\partial^2 u_\theta}{\partial r \partial z} + \frac{2u_r u_\theta}{r} \frac{\partial u_r}{\partial r} \\ + \frac{2u_\theta u_z}{r} \frac{\partial u_r}{\partial z} - \frac{2u_r^2 u_\theta}{r^2} - \frac{u_\theta^3}{r^2} + \frac{u_\theta^2}{r} \frac{\partial u_\theta}{\partial r} \end{array} \right), \tag{1.33}$$

$$u_r \frac{\partial u_z}{\partial r} + \frac{u_\theta}{r} \frac{\partial u_z}{\partial \theta} + u_z \frac{\partial u_\theta}{\partial z} =$$
$$\nu \left(\frac{1}{\partial r} \left(\frac{1}{r} \frac{\partial u_z}{\partial r}\right) + \frac{1}{r^2} \frac{\partial^2 u_z}{\partial \theta^2} + \frac{\partial^2 u_z}{\partial z^2}\right)$$
$$-\lambda_0 \left(u_r^2 \frac{\partial^2 u_z}{\partial r^2} + 2u_r u_z \frac{\partial^2 u_z}{\partial z^2} + \frac{u_\theta^2}{r^2} \frac{\partial u_z}{\partial r} + u_z^2 \frac{\partial^2 u_z}{\partial z^2}\right). \tag{1.34}$$

1.17 Darcy Law

It interprets the flow of a liquid through a spongy medium. This law was originated and dependent on the consequences of analysis on the flow of water across the beds of sand. It additionally models the scientific basis of fluid permeability needed in the Geo sciences.

1.18 Darcy-Forchheimer Law

Movements in spongy medium with Reynolds numbers than 10, and in which inertial effects are prominant. So, this inertial term is add on the Darcys equation and is called as Forchheimer term. This term is able to account for the non-linear behavior of the pressure difference and flow data.

$$\frac{\partial p}{\partial x} = -\frac{\mu}{k}q - \frac{\rho}{k_1}q^2, \tag{1.35}$$

where q represent Forchheimer velocity and the additional term k_1 is known as inertial permeability.

1.19   Hall Effect

When an electrical current passes through a sample in the presence of a magnetic field, a potential proportionate to the current and magnetic field arises across the material in a direction perpendicular to both the current and the magnetic field. This is referred to as Hall current. Edwin Hall, who discovered the phenomenon in 1897, is commemorated with the effect's name.

mathematically

$$F_m = eV_d B, \tag{1.36}$$

where V_d is the drift velocity of the charge.

1.20   Hall current and Ion-slip

$$J = \sigma \left[(\mathbf{E} + (\mathbf{V} \times \mathbf{B})] - \frac{\omega_e \tau_e}{B_o}(J \times B) + \frac{\omega_e \tau_e \beta_i}{B_o^2}(J \times B) \times B, \tag{1.37}$$

where V is the velocity vector, E is the intensity vector of the electric field, τ_e is the electrical collision time, $J = (J_x, J_y, J_z)$, is the current density vector, ω_e is the cyclotron frequency and B is the magnetic field,.

1.21   Gyrotectic Microorganisms

These are the motile microorganisms found in lakes, rivers, and seas. Gayrotectic microorganisms are utilised in experiments because they aid in bio-convective movement. When a significant number of microorganisms congregate on the upper layer of suspension, the layer

becomes thick, and the microorganisms become unstable and begin to move downward, resulting in bio-convection.

1.22 Activation Energy

The base energy required for a chemical response to happen is known as activation energy. This energy depend upon its rate, if the energy is low then the reaction rate is high and vice versa.

1.23 Dimensionless numbers

1.23.1 Reynolds number

It is the most fundamental dimensionless number used to differentiate between different flow characteristics such as laminar and turbulent flow. It represents the ratio of inertial to viscous forces.It is mathematically stated as:

$$\text{Re} = \frac{vL}{\nu}. \tag{1.38}$$

Here, v denotes the velocity of fluid, ν stands for kinematic viscosity, L represents the characteristic length. Different flow regimes within a comparable fluid, such as laminar or turbulent flow are described by Reynolds numbers. At high Reynolds number turbulent flow arise, where inertial forces are dominant. At low Reynolds number laminar flow occurs, where viscous forces are dominant.

1.23.2 Chemical reaction parameter

The non dimensional number used to measure the strength of chemical reaction rate is called Chemical reaction parameter

1.23.3 Prandtl number

Momentum diffusivity to the thermal diffusivity ratio is termed as Prandtl number. Mathematically it can be expressed as::

$$\Pr = \frac{\nu}{\alpha} = \frac{\mu C_p}{k}, \tag{1.39}$$

where C_p denotes the specific heat,thermal diffusivity (α), μ represents the dynamic viscosity, Momentum diffusivity $\nu\prime$, and k stands for thermal conductivity. In heat transfer, the Prandtl number is used to control the thickness of momentum and thermal boundary layers.

1.23.4 Forchheimer number

Pressure gredient to the viscous resistance ratio is described by Forchheimer number. Forchheimer number is proposed to identify flow patterns.

Mathematically

$$Fr = \frac{k^* \rho \nu \beta^*}{\mu}, \tag{1.40}$$

with k^* the permeabity of porous medium and β^* non-Darcian.

1.23.5 Nusselt number

The non-dimension number which represents the convective to conductive heat transfer ratio is known as Nusselt number. Mathematically

$$Nu_L = \frac{h\Delta T}{k\Delta T/L} = \frac{hl}{k}, \tag{1.41}$$

where h stands for convective heat transfer, L for characteristic length and k for thermal conductivity.

1.23.6 Skin friction coefficient

Liquid passing over a surface experiences certain amount of darg that is termed as skin friction. It take place between the flowing liquid and the solid surface that causes reduction in

the rate of flow of fluid. The skin friction coefficient can be defined as:

$$C_f = \frac{\tau_w}{\frac{1}{2}\rho U_w^2},$$

(1.42)

where ρ stands for density, τ_w stands for wall shear stress, and U_w represents the stretching velocity.

1.23.7   Biot number

It can be defined as ratio of internal diffusion resistance to external convection resistance. Mathematically

$$\gamma = \frac{h}{k}\sqrt{\frac{\nu}{a}},$$

(1.43)

where k the thermal conductivity, h the convective heat transfer coefficient ν is the kinematic viscosity,.

1.23.8   Peclet number

Peclet number is interpreted as ratio of transfer of themal energy by fluid movement to transfer of thermal energy by diffusion.

$$Pe = \frac{\text{advective tranfer rate}}{\text{diffusive tranfer rate}}.$$

(1.44)

1.23.9   Thermophoresis parameter

Thermophoresis is a mechanism which is used to prevent the mixing of different particles due to a pressure gradient when they move together or separate the mixture of particles after mixing up. In a cold surface thermophoresis is positive and it is negative for a hot surface.
Mathematically it can be written as:

$$N_t = \frac{(\rho C_p)D_T(T_f - T_\infty)}{(\rho C_f)\,\nu T_\infty},$$

(1.45)

where T_f and T_∞ are the wall temperature and temperature outside the plate, D_T is thermophoretic diffusion coefficient and ν the kinematic viscosity.

1.23.10 Brownian motion parameter

Brownian motion occurs due to size of the nanoparticles in a nanofluid.It is a nanoscale mechanism that displayed the thermal influences of nanofluid.

Mathematically,

$$N_b = \frac{\tau D_B(C_f - C_\infty)}{\nu},$$
(1.46)

where

$$\tau = \frac{\rho C_p}{\rho C_f}.$$
(1.47)

In the above equation ν the Kinematic viscosity. C_w the walls concentration, C_∞ the ambient concentration and and D_B the Brownian diffusion coefficient τ is the ratio of effective heat and heat capacity of the nanoparticles and fluid respectively.

1.23.11 Schmidt number

Schmidt number Sc is defined as the dimensionless quantity which measures the ratio of non-newtonian viscosity (kinematic) to mass diffusivity. It is introduced by Heinrich Wihel Schmidt in $(1892 - 1972)$.

Mathematically

$$Sc = \frac{\nu}{D_B},$$
(1.48)

where ν is kinematic viscosity and D_B is mass diffusivity.

1.23.12 Lewis number

It describes the thermal diffusivity to Browniwn diffusivity

$$Le = \frac{\text{Thermal diffusivity}}{\text{Browniwn diffusivity}}.$$
(1.49)

Molecular diffusivity decreases when Lewis number increases.

1.24　Fundamental laws

The fundamental laws that are used for the flow specification in the subsequential analysis are given below.

1.24.1　Law of mass conservation

Conservation law for mass defines that the whole mass in closed system will remain conserved. Mathematically

$$\frac{D\rho}{Dt} + \rho \boldsymbol{\nabla}.\mathbf{V} = 0, \tag{1.50}$$

or

$$\frac{\partial \rho}{\partial t} + (\mathbf{V}.\boldsymbol{\nabla})\,\rho + \rho\boldsymbol{\nabla}.\mathbf{V} = 0, \tag{1.51}$$

or

$$\frac{\partial \rho}{\partial t} + \boldsymbol{\nabla}.\,(\rho\mathbf{V}) = 0. \tag{1.52}$$

It is known as the equation of continuity. For the steady flow above Eq. (1.52) becomes

$$\boldsymbol{\nabla}.\,(\rho\mathbf{V}) = 0, \tag{1.53}$$

and if the fluid is incompressible then above Eq. (1.52) implies that

$$\boldsymbol{\nabla}.\mathbf{V} = 0. \tag{1.54}$$

1.24.2　Momentum conservation law

It is defined as the total linear momentum of a closed system is constant. Generally, it is given by

$$\rho\frac{D\mathbf{V}}{Dt} = \mathrm{div}\,\boldsymbol{\tau} + \rho\mathbf{b}, \tag{1.55}$$

where $\mathbf{b}$ stands for body force, $\frac{D}{Dt}$ represents the material time derivative and $\boldsymbol{\tau} = -\mathbf{pI} + \mathbf{S}$ denotes the Cauchy stress tensor.

1.24.3   Law of energy conservation

Law of conservation of energy is also known as energy equation and is given by:

$$\rho\frac{D\mathbf{e}}{Dt} = \boldsymbol{\tau}.\mathbf{L} - \boldsymbol{\nabla}.\mathbf{q} + \rho r, \tag{1.56}$$

in which $\mathbf{e}$ stands for specific internal energy, $\mathbf{q}$ for heat flux vector and r for thermal radiation. Energy equation without thermal radiation takes the form:

$$\rho C_p\frac{DT}{Dt} = \boldsymbol{\tau}.\mathbf{L} + k\boldsymbol{\nabla}^2 T, \tag{1.57}$$

where $\mathbf{q} = -k\boldsymbol{\nabla}T$, $\mathbf{e} = C_pT$, T for temperature and k denote the thermal conductivity.

1.24.4   Law of conservation of concentration

For nanoparticles, the volume fraction equation is

$$\frac{\partial C}{\partial t} + \mathbf{V}.\boldsymbol{\nabla}\mathbf{C} = -\frac{1}{\rho_p}\boldsymbol{\nabla}.\mathbf{j}_p, \tag{1.58}$$

$$\mathbf{j}_p = -\rho_p\mathbf{D}_B\boldsymbol{\nabla}\mathbf{C} - \rho_p\mathbf{D}_T\frac{\boldsymbol{\nabla}T}{T_\infty}, \tag{1.59}$$

$$\frac{\partial C}{\partial t} + \mathbf{V}.\boldsymbol{\nabla}\mathbf{C} = \mathbf{D}_B\boldsymbol{\nabla}^2\mathbf{C} + \mathbf{D}_T\frac{\boldsymbol{\nabla}^2 T}{T_\infty}. \tag{1.60}$$

Here, $\mathbf{D}_T$ thermophoretic coeffcients, C nanoparticle concentration, T temperture, $\mathbf{D}_B$ Brownian diffusivity.

1.25   Thermal diffusivity

It is the measurment of the capacity of a substance to conduct heat. This value describes how speedily a material respond to change in temperature. It is ratio of thermal conductivity to the product of specific heat capacity and density. Mathematically

$$\alpha = \frac{\kappa}{\rho C_p}, \tag{1.61}$$

where κ indicates the thermal conductivity, C_p the soecific heat capacity and ρ the density.

1.26 Thermal conductivity

The measurement of the capability of a material to conduct heat is defined as thermal conductivity. Acoording to Fourier Law of heat conduction, it is defined as " the amount of heat transfer rate (Q) through a material of unit thickness (L) times unit cross section area (A) and unit temperature difference (ΔT)". Mathematically, written as:

$$k = \frac{QL}{A(\Delta T)}. \tag{1.62}$$

In SI system thermal conductivity has unit $\frac{W}{m.K}$ and dimension is $\left(\frac{ML}{T^3\theta}\right)$.

Chapter 2

INTRODUCTION AND LITERATURE REVIEW

Nanofluids have show some amazing uses in different fields of research, including chemical and biomechanics, thermal engineering, industrial technology and nuclear industries. Because of the reduction in size, microscopic devices are subjected to significant heat loads that need effective and speedy removal throughout their working life. Water, ethylen glycol these are conventianal base fluids and themal conductivity of these fluid is very poor. To enhance the thermal conduectivity of these fluid we add some nanoparticles in it with nanoparticle volume fraction is less then one percent. Choi and aestman [1] pitched the idea of nanofluids in 1995. Buongiorno [2] later reconnoitre the nanofluid convective transport by including thermophoresis characteristics and Brownian motion. According to this study, the absolute velocity of nanofluid may be expressed as the sum of the base fluid and relative slip velocities. Thermophoresis characteristics and Brownian motion play a critical part in Buongiorno nanofluid model, out of seven slip variables for heat transmission. Unlike base fluids, motile bacteria may be moved using the thermophoresis characteristics and Brownian motion. Few scientists collaborated on Buongiorno's nanofluid model to better understand heat exchange improvement in natural heat dissipation convection in nanofluids. Fetecau et al. [3], investigated the natural convection flow of a nanofluid by an isothermal moving surface. Brownian motion and thermophoresis effects for Williamson flow of nanofluid induced by stretched configuration were deliberated

by Bhatti and Rashidi [4]. Turkyilmazoglu [5] discussed nanofluid interaction in a jet flow. Venthan et al. [6] investigated the use of Bingham nanofluids by cylindrical rings caused by a rortating inner cylinder. Waqas et al. [7] investigated the nanofluid analysis for Maxwell-based micropolar with slip effects and porous medium. Ali et al. [8] established heat transfer a contacting and extending cylinder using cross nanofluids and magnetic force. Ghalambaz et al.[9] used encapsulated phase change materials to conceptually address thermal transfer studies in a porous region. Rafiq et al. [10] provided analysis of nanomaterials and their novel applications in a variety of physicochemical systems. References [11 − 15] provide some further interesting papers describing the thermal characteristics of nanomaterials.

Another inquisitive area of research is the flow configured by extending and rotating disks, which involves novel applications in industries such as injection modelling,thrust bearings, semiconductor manufacturing, lubrications, compression, polymer processing, rotating electrodes, viscometry, aircraft engines, geothermal, rotating wafers, power transmission,centrifugal pumps, turbine engines, mechanical components transient loading, storage devices for computers, medical equipment, steam and microclimate systems, etc. A few applications of stretching geometries include plastic and rubber sheet production, the new rolling wire drawing, the vehicle manufacturing business, glass fibre production, big sized cooling plates in bath tubs.Von Karman [16] identified the flow changes caused by spinning disks. Researchers are still interested in the stretching disk in fluid flow for viscous and viscoelastic fluids. Flow within/through stretching disk, surfaces, plates, and stretching boundaries has a significant influence on industrial and technical applications. Turkyilmazoglu [17] investigated the flow of viscous fluid caused by an infinitely spinning disk in the presence of magnetic force. Khan et al. [18] used chemical reaction to guide the chemically reactive flow of Maxwell liquid between stretching disks. Karman [19] investigates the fundamentals of flow on a spinning infinite disk. Cochran [20] used the Von Karman transformation. Benton [21] discusses the exact solution for transient flow past a spinning disk. Using the bvp Midrich approach, Hafeez et al. [22] quantitatively examined the impact of homogeneous heterogeneous (h–h) reaction on Oldroyd-B fluid moving across a spinning disk.

Non-Newtonian fluids play an essential role in many industrial liquids including plastics, polymers, pulps, toothpaste, and fossil fluids. A number of models have been proposed to simu-

24

late the analysis of these liquids. Fluids with non-Newtonian behaviour have been employed in a variety of technical applications, including remediation, hydraulic fracturing and a variety of industrial processing. When compared to Navier–Stokes equations, the equations of motion of non-Newtonian fluids are highly nonlinear. Non-Newtonian fluid models are classified into three types: rate type, integral, and differential type. Shear stress and shear rate are inextricably related in non-Newtonian liquids due to their nonlinear nature. The fluid model under consideration here is a sub-category of a rate type fluid known as Maxwell fluid. The Maxwell fluid model predicts the effects of relaxation time. These effects cannot be projected by any other fluid form. Maxwell nanofluid flow over a rotating disk has piqued the scholars' interest due to its numerous applications in engineering and innovation. The most fundamental viscoelastic fluid model is the Maxwell flow regime, which expresses memory effects through fluid relaxation time Ahmed et al. [23] investigated the flow of Maxwell fluid driven by gyrating disks while accounting for mixed convection and Karman whirling flow of Maxwell fluid. Khan et al. [24] studied the Maxwell fluid flow through a smooth moving gyrating disks under the impact of radiation and magnetic impact. Ijaz and Ayub [25] investigated the effect of activation energy on stratification Maxwell fluid flow with suspended nanoparticles. The Casson fluid model stands out with its uniqueness aspects. The rheological behavior of viscoelastic fluids are described using this model. Shear thinning fluid is the term used to describe this condition. Casson fluid may be found in a variety of forms, concentrated fruit juice, blood, including jelly, tomato sauce and honey. Khan et al. [26] analyzed the Lorentz force influence on a non-linear radiative Casson fluid flow including gold nano particles. According to the findings of this study, when increased the velocity ratio parameter, the radial direction of fluid velocity is enhanced. Khan et al. [27] provided a computer solution for an electrical conductor axisymmetric radiative Casson nanofluid in a porous channel interacting chemically with two deformable disks.

Hall current and Ion-slip is induced when the strong magnetic field is applied normally to the flow of the current. Due to this,

Ohm's law is modified. Nanofluid flow analysis with MHD and Hall/Ion slip current is an important application in both science and engineering. Jana and Datta [28] investigated the Hall effects on MHD flow caused by torsional oscillations of a disk in a rortating environment. Datta [29] investigated the effects of Hall current on the torsional oscillations of a disk in a

conducting fluid exposed to a symmetric axial magnetism. Heat transfer is MHD flow with Ion-slip and Hall currents is explored by Mittal and Bhat [30]. Abo-Eldahab et al. [31] studied the combined effects of Ion-slip and Hall current on MHD free convective heat producing flow across a semi infinite vertical flat plate. Attia [33] investigated the transient MHD fluid motion with heat transfer while accounting for ion-slip. Attia [32, 34] also studied the combined effects of Ion-slip and Hall current in a conducting fluid flow caused by a rortating disk. Guria et al. [35] studied the effects of Hall current and Ion slip state on the unsteady viscous incompressible fluid due to the non rotation of a porous disk. Ghara et al[36]. investigated the effects of Hall current and Ion-slip on MHD flow caused by torsional oscillations of a disk in a rotating fluid.

Heat is conveyed in a fluid flow by two mechanisms: first when thermal conductivity plays a vital role in increasing the random movement among the molecules and second when the collision between molecules increases. Thermal conductivity is used extensively in steam electrolytes, generators, and laminating. Rafiq et al. [37] investigated a numerical solution for a permeable rotating disk with rotational flow time-dependent and fluid characteristics depended on temperature. For increasing values of the variable viscosity parameter, there is a little increase in the rate of heat transfer rate. Khan et al. [38] examined the impact of thermophysical properties of gases and liquids in a three-dimensional flow through a rotating disk. Fifth-order Runge–Kutta quadrature is used for numerical integration of the problems. In this study, a significant surge in the temperature field is seen when the variable thermal conductivity is increased. Ahmed et al. [39] investigated the effect of a sink/heat source on Maxwell fluid mixed with changing thermal conductivity on a radially deformable rotating disk using the Boungirono model. Here, the rate of heat transmission is shown to increase as the rotating and stretching ratios are increased. Referances [40−41] demonstrate extensive research on deformable surface with a variety of physical properties.

Bioconvection is the spontaneous pattern development in the swimming microorganisms. like natural convection, bioconvection occurs due to the unstable stratification, *i.e.*, it is caused by the up swimming of microorganisms like algae which form a concentrated layer on the upper surface of the fluid. Microorganisms are slightly denser than water. Generally, the microorganisms swim upwards and the reason for up swimming is different for different species . The stimulator which tends the self-propelled microorganisms to swim in particular direction

include an oxygen concentration gradient. Amongst these movements, some are gravitaxis, chemotaxis, gyrotaxis and phototaxis. The movement microorganisms is in the opposite direction to gravity up a chemical gradient and toward or away from light. Gyrotaxis is controlled by the torque due to gravity and viscous shear forces on bottom-heavy cells (some algae and bacteria), so in gyrotaxis, the cells tend downwelling fluid. Microorganisms that are involved in the bioconversion phenomenon are the bottom-heavy algae (Chalamydomonas nivalis) and common soil bacterium (B. subtilis). Abdelmalek et al [42] investigated the numerical solution of the rate type thin film nanofluid flow over a rotating disk with bioconvection, activation energy, and Ohmic heating. When the buoyancy ratio parameter is increased, axial and tangential velocities are decreased, according to the above investigation. Kuznetsov [43] directed the leading continuation on this topic, for which a range of extensions with varied flow geometries and unique properties have been proposed in recent days [45 − 49].

Many natural physical processes can be interpreted by variable viscosity. Temperature-dependent viscosity is used to character the thermophysical properties of liquids and gases. Rafiq et al. [50] investigated variable thermophysical properties of nanofluid flow in a decelerating spinning disk. Ahmad et al [51] showed that the thickness of the boundary layer is reduced by increasing the value of thermally radiative flow across a permeable rotating disk. Numerous researchers are now conducting studies to investigate the impact of variable viscosity employing a variety of physical implications.[52 − 53]. Among the thermo physical propertyties of the fluid, studying the effect the thermal conductivity is inevitable. Many engineering and various physical processes are based on temperature-dependent thermal conductivity. Many authors have pointed out the flow phenomenon by considering temperature-dependent thermal conductivity. Khan et al. [54] investigated the variable thermal conductivity of liquid and gases near the rotating disk. Ahmad et al. [55] addressed the Maxwell fluid flow for variable features.

The goal of this thesis is investigate significance of Hall current and Ion slip in a three dimensional Maxwell nanofluid flow over rotating disk with variable charateristics. In additional, we studied Hall and ion slip effects, Maxwell bio-convective nanofluid, and variable viscosity. Partial differential equations are converted to ordinary differential equations using similarity factors, which are the numerically solved using the bvp4c approach

Chapter 3

IMPACT OF A THREE-DIMENSIONAL CASSON NANOFLUID FLOW PAST A ROTATING DEFORMABLE DISK WITH VARIABLE CHARACTERISTICS AND HALL CURRENT

In this chapter, we shall study the influence of variable thermal conductivity, variable mass diffusion and Hall current, a deformable rotating disk which stretched in the radial direction in a 3D-Darcy–Forchheimer–Casson nanofluid flow. The mass flux, activation energy and Cattaneo–Christov heat flux with a chemical reaction are considered here. The model's uniqueness is improved by addition of momentum slip and convective boundary conditions. Using Von karmann similarities transformation are used to convert the partial differential equations

28

into the ordinary differential equations. The bVP4c function in MATLAB provides a numerical solution for a system of differential equations. To substantiate the envisioned problem, a comparison of the current investigation with existing published research is included.

3.1 Mathematical Formulation

Here we consider steady three dimensional incompressible Darcy-Forchheimer Casson nanofluid flow past a rorating deformable disk . The disk is centred at $z = 0$ and rotates at a constant angular velocity Ω. The flow of fluid is axisymmetric and takes place in the $z \geq 0$ of a disk and the disk stretching in the radial direction. The flow is caused due to stretching and rotation of the disk. Magnetic field is applied along the z-direction. The geometry of the problem in cylindrical coordinates is illustrated in Fig.3.1. The impacts of the variable thermal conductivity, thermal radiation, and Cattaneo–Christov $(C-C)$ model are investigated in order to improve heat transfer. In addition, convective heat, mass condition, the effects of velocity slip factor, chemical reactions, variable molecule diffusivity with activation energy are used to investigate the flow. The grverning set of equtions is given as under:
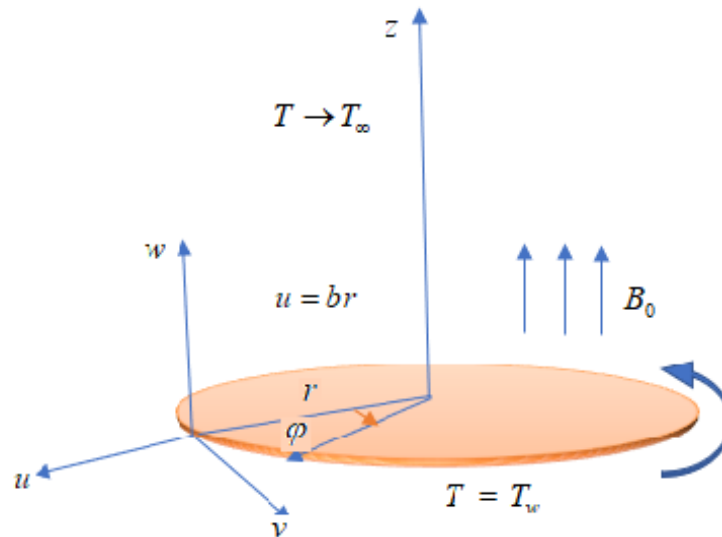

Fig. 3.1 Schematic illustration of the flow.

$$\frac{\partial u}{\partial r} + \frac{u}{r} + \frac{\partial w}{\partial z} = 0, \tag{3.1}$$

$$u\frac{\partial u}{\partial r} - \frac{v^2}{r} + w\frac{\partial u}{\partial z} = \nu\left(1 + \frac{1}{\beta}\right)\left(\frac{\partial^2 u}{\partial r^2} + \frac{1}{r}\frac{\partial u}{\partial r} - \frac{u}{r} + \frac{\partial^2 u}{\partial z^2}\right)$$
$$- \frac{\sigma\beta_0^2}{\rho(1+m^2)}(u - mv) - \frac{\nu}{k^*}u - Fu^2, \tag{3.2}$$

$$u\frac{\partial v}{\partial r} + \frac{uv}{r} + w\frac{\partial v}{\partial z} = \nu\left(1 + \frac{1}{\beta}\right)\left(\frac{\partial^2 v}{\partial r^2} + \frac{1}{r}\frac{\partial v}{\partial r} - \frac{v}{r^2} + \frac{\partial^2 v}{\partial z^2}\right)$$
$$- \frac{\sigma\beta_0^2}{\rho(1+m^2)}(v + mu) - \frac{\nu}{k^*}v - Fv^2, \tag{3.3}$$

$$u\frac{\partial T}{\partial r} + w\frac{\partial T}{\partial z} + \lambda_1\left[\begin{array}{c} u^2\frac{\partial^2 T}{\partial r^2} + 2uw\frac{\partial T}{\partial z \partial r} + w^2\frac{\partial^2 T}{\partial z^2} + u\frac{\partial w}{\partial r}\frac{\partial T}{\partial z} \\ +u\frac{\partial u}{\partial r}\frac{\partial T}{\partial r} + w\frac{\partial u}{\partial z}\frac{\partial T}{\partial r} + w\frac{\partial w}{\partial z}\frac{\partial T}{\partial z} \end{array}\right] =$$
$$\frac{1}{\rho C_p}\frac{\partial\left(K(T)\frac{\partial T}{\partial z}\right)}{\partial z} + \tau D_B\left[\left(\frac{\partial T}{\partial r}\frac{\partial C}{\partial r} + \frac{\partial T}{\partial z}\frac{\partial C}{\partial z}\right) + \frac{D_T}{T_\infty}\left(\left(\frac{\partial T}{\partial r}\right)^2 + \left(\frac{\partial T}{\partial z}\right)^2\right)\right]$$
$$+ \frac{1}{\rho C_p}Q_1\left(T - T_\infty\right), \tag{3.4}$$

$$u\frac{\partial C}{\partial r} + w\frac{\partial C}{\partial z} + \lambda_2\left[\begin{array}{c} u^2\frac{\partial^2 C}{\partial r^2} + 2uw\frac{\partial^2 C}{\partial r \partial z} + w^2\frac{\partial^2 C}{\partial z^2} + u\frac{\partial C}{\partial r}\frac{\partial C}{\partial r} \\ +u\frac{\partial u}{\partial r}\frac{\partial C}{\partial r} + w\frac{\partial u}{\partial z}\frac{\partial C}{\partial r} + w\frac{\partial w}{\partial z}\frac{\partial C}{\partial z} \end{array}\right] =$$
$$\frac{\partial}{\partial z}\left(D_B\left(C\right)\frac{\partial C}{\partial z}\right) + \frac{D_T}{T_\infty}\left(\frac{\partial^2 T}{\partial r^2} + \frac{1}{r}\frac{\partial T}{\partial r} + \frac{\partial T^2}{\partial z^2}\right) - k_r^2\left(C - C_\infty\right)\left(\frac{T}{T_\infty}\right)^n\exp\left(\frac{-E}{kT}\right), \tag{3.5}$$

with boundary conditions are defined as follows:

$$\text{At } \xi = 0 \; u = rb + s\left(1 + \frac{1}{\beta}\right)\frac{\partial u}{\partial z}, \qquad v = r\Omega + s\left(1 + \frac{1}{\beta}\right)\frac{\partial v}{\partial z}, \quad w = 0,$$
$$-K\left(T\right)\frac{\partial T}{\partial z} = h_1\left(T_w - T\right), \qquad -D_B\left(C\right)\frac{\partial C}{\partial z} = h_2\left(C_w - C\right), \tag{3.6}$$
$$\text{as } \xi \to \infty \; u \longrightarrow 0, \qquad v \to 0, \qquad T \to 0, \qquad C \to C_\infty.$$

thermal conductivity varies with temperature

$$K\left(T\right) = k_\infty\left[1 + d\left(\frac{T - T_\infty}{T_w - T_\infty}\right)\right]. \tag{3.7}$$

The variable molecule diffusivity is given as

$$D_B(C) = D_{B_\infty}\left[1 + e\left(\frac{C - C_\infty}{C_w - C_\infty}\right)\right]. \tag{3.8}$$

30

Using appropriate transformation

$$
\begin{aligned}
u &= \Omega r f\left(\zeta\right), v = \Omega r j(\zeta), w = \left(\Omega r\right)^{0.5} h(\zeta), \\
\theta\left(\zeta\right) &= \frac{T + T_\infty}{T_w - T_\infty}, \phi\left(\zeta\right) = \frac{C - C_\infty}{C_w - C_\infty}, \zeta = \left(\frac{\Omega}{v}\right)^{\frac{1}{2}} z.
\end{aligned}
\tag{3.9}
$$

Here Eqs. $(3.1 - 3.5)$ take the form

$$
2f\left(\zeta\right) + h f^{'}\left(\zeta\right) = 0,
\tag{3.10}
$$

$$
\begin{aligned}
&\left(1 + \tfrac{1}{\beta}\right).f''\left(\zeta\right) - \left(\lambda + Fr.f\left(\zeta\right)\right) f\left(\zeta\right) - \\
&\tfrac{Ha^2}{1+m^2}\left(f\left(\zeta\right) - m.j\left(\zeta\right)\right) - f^{\,2}\left(\zeta\right) + j^2\left(\zeta\right) - f^{'}\left(\zeta\right).h\left(\zeta\right) = 0,
\end{aligned}
\tag{3.11}
$$

$$
\begin{aligned}
&\left(1 + \tfrac{1}{\beta}\right).j''\left(\zeta\right) - \left(\lambda + Fr.j\left(\zeta\right)\right).j\left(\zeta\right) \\
&-\tfrac{Ha^2}{1+m^2}\left(h\left(\zeta\right) + m.f\left(\zeta\right)\right) - 2f\left(\zeta\right).j\left(\zeta\right) - h\left(\zeta\right).j'\left(\zeta\right) = 0,
\end{aligned}
\tag{3.12}
$$

$$
\begin{aligned}
&\left(1 + d_1.\theta\left(\zeta\right)\right) - k_1.\Pr.h\left(\zeta\right).\theta''\left(\zeta\right) + d_1.\left(\theta'\left(\zeta\right)\right)^2 + \Pr. \\
&\left[\begin{array}{c} N_b.\theta'\left(\zeta\right).\phi\left(\zeta\right) + N_t.\left(\theta'\left(\zeta\right)\right)^2 + Q^*.\theta\left(\zeta\right) \\ -h\left(\zeta\right).\theta'\left(\zeta\right) - K_1.h\left(\zeta\right).h'\left(\zeta\right).\theta'\left(\zeta\right) \end{array}\right] = 0,
\end{aligned}
\tag{3.13}
$$

$$
\begin{aligned}
&\left(1 + e\phi\left(\zeta\right) + K_2.S_c.h^2.\left(\zeta\right)\right).\phi''\left(\zeta\right) + e.\left(\phi'\left(\zeta\right)\right)^2 \\
&+N_t\tfrac{1}{N_b}\theta''\left(\zeta\right) - S_c\left[\begin{array}{c} h\left(\zeta\right).\phi'\left(\zeta\right) + K_2.h\left(\zeta\right).h'\left(\zeta\right).\theta'\left(\zeta\right) \\ +\delta.\phi\left(\zeta\right)\left(1 + \alpha.\theta\left(\zeta\right)\right)^n \exp\left(\tfrac{-E}{1+\alpha\theta(\zeta)}\right) \end{array}\right] = 0,
\end{aligned}
\tag{3.14}
$$

boundary conditions

$$
\begin{aligned}
\text{At } \zeta = 0 \; & f\left(0\right) = p + L\left(1 + \tfrac{1}{\beta}\right) f'\left(\zeta\right), j\left(0\right) = 1 + L\left(1 + \tfrac{1}{\beta}\right) j'\left(\zeta\right), h\left(0\right) = 0, \\
& \theta'\left(\zeta\right) = -H_1\left(\tfrac{1-\theta(0)}{1+f.\theta}\right), \phi'\left(\zeta\right) = -H_2\left(\tfrac{1-\phi(0)}{1+e\phi}\right), \\
\text{As } \zeta \longrightarrow \infty \quad & f \to 0, g \to 0, \theta \to 0, \phi \to 0.
\end{aligned}
\tag{3.15}
$$

The expression for non-dimensional parameter given in equations $(3.11) - (3.15)$ are ;

$$
\begin{aligned}
\Pr &= \frac{\mu c_p}{k_\infty}, N_b = \frac{\tau D_B \left(C_w - C_\infty\right)}{v}, N_b = \frac{\tau D_T \left(T_w - T_\infty\right)}{v T_\infty}, E = \frac{E_a}{kT}, L = S \sqrt{\frac{\Omega}{v}}, \\
K_1 &= \lambda_1 \Omega, K_2 = \lambda_2 \Omega, H_1 = \frac{h_1}{k_\infty} \sqrt{\frac{v}{\Omega}}, H_2 = \frac{h_2}{k_\infty} \sqrt{\frac{v}{\Omega}}, Q^* = \frac{Q_1}{\rho c_p \Omega}, \delta = \frac{k_r^2}{\Omega}, \\
\lambda &= \frac{v}{k^* \Omega}, \alpha = \frac{T_w - T_\infty}{T_\infty}, Ha = \frac{\sigma B_0^2}{\rho \Omega}, F_r = \frac{c_b^*}{\sqrt{k^*}}, P = \frac{b}{\Omega}, \mathrm{Re} = \frac{\Omega}{v} r^2, \quad (3.16)
\end{aligned}
$$

where $\lambda, Fr, \alpha, Nt, H_1, H_2, \Pr, Sc, Nb, e, k_1, k_2, \delta, S, E, P, L, m, Ha, H_1, d_1, Q^*$ are local porosity parameter, Forcheimer number, Temperature ratio parameter, Thermophoresis parameter, heat transfer Biot number, Mass transfer Biot number, Prandtl number, Schmidt number, brownian motion parameter, variable molecular diffussivity, thermal relaxation parameter, concentration relaxation parameter, Activation energy parammeter, stretching parameter, velocity slip parameter, Hall current parameter, magnetic parameter, thermal relaxation parameter, variable thermal conductivity, and heat source parameter to the angular velocity respectively.

The wall shear stress (drag force coefficient), heat transfer rate Nu_r, and mass transfer Sh_r are defined as follows:

$$
C_f = \left(1 + \frac{1}{\beta}\right) \frac{\tau_w}{\rho \left(r\Omega\right)^2}, \qquad \tau_w = \left(\tau_{rz}^2 + \tau_{z\theta}^2\right)^{\frac{1}{2}}, \qquad (3.17)
$$

$$
\text{where} \quad z = 0 \qquad \tau_{rz}^2 = \mu \frac{\partial u}{\partial z}, \qquad \tau_{z\theta}^2 = \mu \frac{\partial v}{\partial z}.
$$

$$
Nu_r = \frac{r Q_w}{K_\infty \left(T_w - T_\infty\right)}, \qquad Q_w = -K\left(T\right) \frac{\partial T}{\partial z}. \qquad (3.18)
$$

$$
Sh_r = \frac{r Q_m}{D_{B_\infty} \left(C_w - C_\infty\right)}, \qquad Q_m = -D_B \frac{\partial C}{\partial z}. \qquad (3.19)
$$

By utillizing Eqs. (3.9) in Eqs. $(3.17), (3.18), (3.19)$ are transmuted. Dimensionless forms of Skin friction and local Nusselt number are appended as follows:

$$
C_r \mathrm{Re}_r^{\frac{1}{2}} = \left(1 + \frac{1}{\beta}\right) \left[\left(f\left(\zeta\right)\right)^2 + \left(j\left(\zeta\right)\right)^2\right]^{\frac{1}{2}}, \qquad (3.20)
$$

$$
Nu_r \mathrm{Re}_r^{\frac{1}{2}} = -\left[1 + d_1 \theta\left(\zeta\right)\right] \theta\left(\zeta\right), \qquad (3.21)
$$

$$Sh_r \operatorname{Re}_r^{\frac{1}{2}} = -\left[1 + e\phi\left(\zeta\right)\right]\phi\left(\zeta\right). \tag{3.22}$$

3.2 Numerical procedure

The coupled nonlinear Ordinary differential equations (ODEs) are numerically calculated using MATLAB's bvp4c function. Higher-order differential equations are reduced to first-order equations. Step size $h = 0.01$ is considered with the tolerance10^{-6}. The converssion of higher order ODE to is ODE of oder one is given as under:

$$
\begin{aligned}
f\left(\zeta\right) &= y_1, f'\left(\zeta\right) = y_2, f''\left(\zeta\right) = yy_1, j\left(\zeta\right) = y_3, \\
j'\left(\zeta\right) &= y_4, j''\left(\zeta\right) = yy_2, h\left(\zeta\right) = y_5, h'\left(\zeta\right) = yy_3.
\end{aligned} \tag{3.23}
$$

Using Eqs. (3.23) is in Eqs. $(3.10),(3.11),(3.12)$

$$yy_1 = \frac{1}{\left(1 + \frac{1}{\beta}\right)}\left[\lambda y_1 + Fr\left(y_1\right)^2 + \frac{(Ha)^2}{(1+m^2)}\left(y_1 - my_3\right) + \left(y_2\right)^2 - \left(y_3\right)^2 + y_2.y_5\right], \tag{3.24}$$

$$yy_2 = \frac{1}{\left(1 + \frac{1}{\beta}\right)}\left[\lambda y_3 + Fr.\left(y_3\right)^2 + \frac{(Ha)^2}{(1+m^2)}\left(y_3 - my_1\right) + 2y_1.y_3 + y_4.y_5\right], \tag{3.25}$$

$$yy_3 = -2.y_1, \tag{3.26}$$

$$\theta\left(\zeta\right) = y_6, \theta'\left(\zeta\right) = y_7, \theta''\left(\zeta\right) = yy_4, \phi\left(\zeta\right) = y_8, \phi'\left(\zeta\right) = y_9, \phi''\left(\zeta\right) = yy_5, \tag{3.27}$$

Using equaion (3.27) in equestions (3.13) and (3.14), we get

$$yy_4 = \frac{1}{\left(\left(1 + d_1 y_6\right) - K_1 \operatorname{Pr}.\left(y_5\right)^2\right)}\left[-d_1.\left(y_7\right)^2 - \operatorname{Pr}\left\{\begin{array}{l} N_b.y_7.y_9 + N_t.\left(y_7\right)^2 + \\ Q^*.y_6 - y_5 y_{7-K_1.y_5.yy_3.y_7} \end{array}\right\}\right], \tag{3.28}$$

$$yy_5 = \frac{1}{\left(\left(1 + e.y_8\right) - K_2 S_c.\left(y_5\right)^2\right)}\left[\begin{array}{l} -e\left(y_9\right)^2 - \frac{N_t}{N_c}.yy_4 + \\ S_c\left(\begin{array}{l} \delta.y_9\left(1 + \alpha.y_5\right)^n \exp\left(\frac{-E}{1+\alpha.y_6}\right) \\ +y_5.y_9 + K_2.y_5.yy_3.y_9 \end{array}\right) \end{array}\right]. \tag{3.29}$$

The boundary conditions are:

At $\zeta = 0$, $y_1(0) = p + L\left(1 + \frac{1}{\beta}\right)y_2(0)$, $y_3(0) = 1 + L\left(1 + \frac{1}{\beta}\right)y_4(0)$,

$$y_5(0) = 0, \quad y(0) = -H_1\left(\frac{1-y_6}{1+d.y_6}\right), y_9(0) = -H_2\left(\frac{1-y_8}{1+ey_8}\right), \tag{3.30}$$

As $\zeta \to \infty$ $\quad y(\infty) \to 0, y(\infty) \to 0, y(\infty) \to 0, y(\infty) \to 0$.

3.3   Results and discussion

The effects of nondimensional parameters against included profiles in the a highly nonlinear mathematical model is graphically investigated. Figs. $3.2 - 3.7$ show that of relevant factors on the velocity radial field $f(\zeta)$, tangential field $j(\zeta)$, and axial field $h(\zeta)$. Figs. $3.2a$, and $3.2b$, display the effect of magnetic field parameter Ha on $f(\zeta)$ and $j(\zeta)$. It is observed for higher estimatios of Ha the $f(\zeta)$ and $j(\zeta)$ are decrecsing because Lorentz force is stronger. which causes resistance to fluid. Figs. $3.3a$ and $3.3b$ show the effects of the Casson fluid parameter β on $f(\zeta)$ and $j(\zeta)$. The velocity profile decline for greater Casson fluid parameter (β) because β is the ratio of dynamic viscosity to yield stress. when yield stress is increasing away from the surface, the Casson fluid parameter β is declined, that is why velocity profiles decreas. Figs. $3.4a$ and $3.4b$ reveal the effect of Darcy parameter (F_r) on $f(\zeta)$ and $j(\zeta)$. It is noticed that velocity profile lessening for mounting F_r. because for higher F_r causes resistance due to the resistance in fluid motion that's why velocity of liquid decline. The effect of the porosity parameter λ on $f(\zeta)$ and $j(\zeta)$ is seen in Fig $3.5a$ and $3.5b$. The kinematic viscosity of fluid increases as the value of increases λ. As a resistance is accelerated that is why $f(\zeta)$ and $g(\zeta)$ become decclined. Figs. $3.6a$ and $3.6b$ represent the behaviour of Hall's current strategic m on $f(\zeta)$ and $j(\zeta)$. The effective conductivity $\frac{\sigma}{1+m^2}$ reduces when m is amplified. An outcome of the magnetic dampening force's effect is decreased. As a result, the fluid velocity $f(\zeta)$ is increased, as shown in Fig. $3.6a$. In $Eq.\,(3.12)$, by increasing m, $\frac{1}{1+m^2}$ falls in the condition $\frac{(g+mf)}{1+m^2}$, while $f(\zeta)$ rises. $f(\zeta)$ also has a larger influence than $1 + m^2$. Thus, $j(\zeta)$ reduces as shown in Fig. $3.6b$. The effect of velocity slip parameter L on $f(\zeta)$ and $j(\zeta)$ is depicted in Figs. $3.7a$ and $3.7b$. It has been observed that when the value of L increases, the friction force increases. As a result, more liquid passes through the deformable rotating disk. That is why the fluid flow in $f(\zeta)$ and $j(\zeta)$ dereases. Fig. 3.8 shows the effect of the thermophoresis parameter N_t on $\theta(\zeta)$. The

34

thermophoretic force of nanoparticles is intensified by increasing N_t and nanoparticles travel from hot to cool fluid. As a result,θ (ζ) increasing. The effect of the Brownian motion variable Nb on $\theta(\zeta)$ is shown in Fig. 3.9. Because the collision of the nanoparticles increases as the value of N_b increases, additional heat is created. It is concluded that $\theta(\zeta)$ increases as N_b increases. The impact of heat production and absorption parameter (Q^*) on $\theta(\zeta)$ is seen in Figs. 3.10a and 3.10b. It is observed that when Q^* is agumented, a large amount of heat is produced. As a result, the system agains more heat. So, the thermal field expands, For the negtive value Q^* it shows oppsitive behavior. As a result, the thermal profile decreases. The impact of the Prandtl number Pr on $\theta(\zeta)$ is seen in Fig. 3.11. Since by increasing Pr, the fluid's viscosity increases, while heat diffusion decreases. As a result, heat dissipation from the heated surface decreases. Fig. 3.12 show the increasing effect for different value of d_1 on $\theta(\zeta)$. As the value of d_1 increases, the collision between the nanoparticles becomes more intense, and more heat is transferred through the fluid. Fig. 3.13 reveal the effect of heat transfer Biot number (H_1) on $\theta(\zeta)$. For increasing values of H_1 heat transfer coefficient improves. It is understood that $\theta(\zeta)$ intensifies rapidly for increasing H_1. In Fig. 3.14, the effect of increasing thermal relaxation parameter K_1 on $\theta(\zeta)$ is highlighted. On increasing K_1, it is observed that more time is required for the transfer of heat from the heated surface to the fluid. As a result, $\theta(\zeta)$ decreases. In Fig. 3.15, the effect of changing Schmidt number Sc on the concentration profile $\phi(\zeta)$ is explained. It is noticed that when Sc increases, the Brownian motion parameter decreases and the fluid's concentration is decreased. The effect of the chemical reaction parameter (δ) on $\phi(\zeta)$ is depicted in Figs. 3.16a and 3.16b. The annihilation procedure accelerates as δ rises, causing liquid species to dissolve more effectively. As a result, there is δ drop in concentration. Fig. 3.17 shows the of increasing effect of activation energy E. It is observed that when the value of E increases, the kinetics function decreases. As a result, the producing chemical process slows down. As E rises, the fluid concentration rises as well. Fig. 3.18 reveal the effect of mass transfer Biot number (H_2) on $\phi(\zeta)$. For increasing values of H_2 mass transfer coefficient improves. It is understood that $\phi(\zeta)$ intensifies rapidly for increasing H_2. In Fig. 3.19. the effect of increasing the concentration relaxation parameter (K_2) on $\phi(\zeta)$ is shown.It has been shown that when K_2 increases, more time is required for particles diffusion. As a result, increased K_2. Table 3.1 shows the effect of calculated values of non - dimensional parameters Ha, λ and p on the

skin friction coefficient $C_f \, Re_r^{0.5}$. Shear stress is increased with changing P, Ha, and λ. Table 3.2 represents the effect of $Nt, H_1, Pr,$ and d on the local Nusselt number. The rate of heat transmission is to be increasing as Pr and H_1 values increase. $NurRe_r^{0.5}$, on the other hand, decreases at increasing values of Nt and d. Table 3.3 shows the effect of various values of $Sc, e, , H_2, \delta$ and E the local Sherwood number. The rate of mass transfer increases as Sc, δ and H_2 ; however, when e and E increase, the nature of the transfer deteriorates. Table 3.4 shows a comparison of the current work with Hafeez et al. [58], Yin et al. [57], and Turkyilmazoglu [56]. There is a strong correlation between the outcomes.
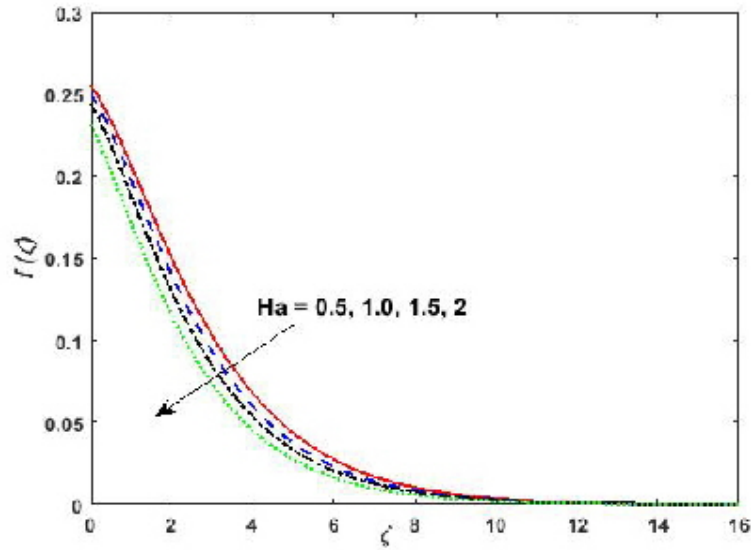
Fig. 3.2(a) Change in β on $f\left(\zeta\right)$
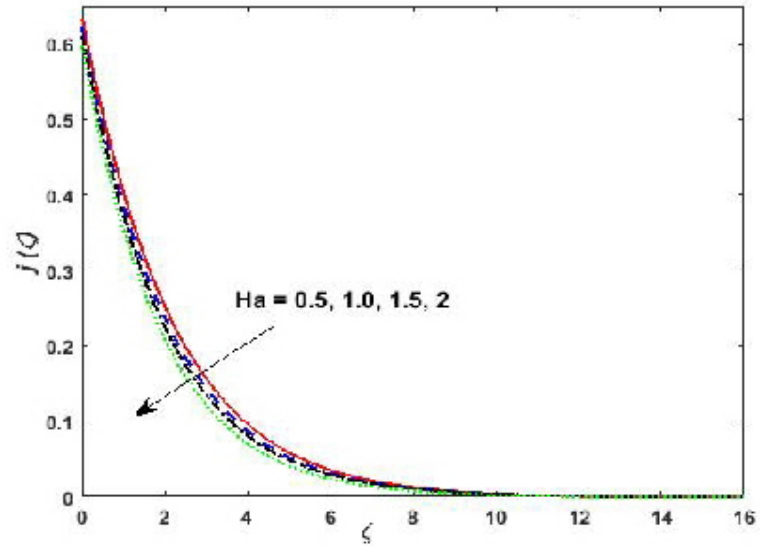
Fig. 3.2 (b) Change in β on $j(\zeta)$

Fig. 3.3 (a) Change in β on $f(\zeta)$

37
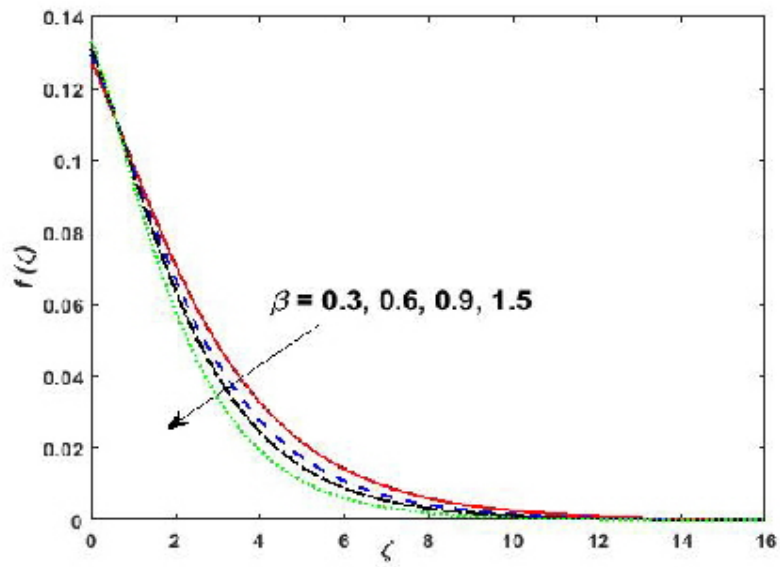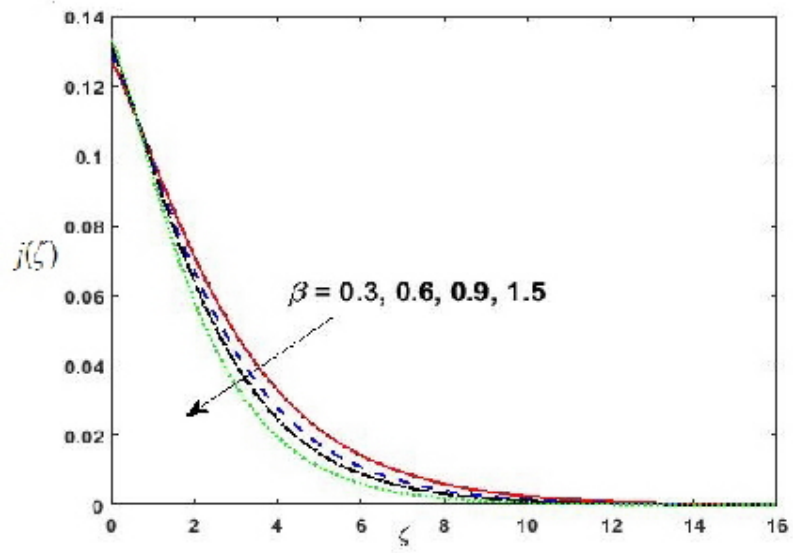
Fig. 3.3 (b) Change in β on $j(\zeta)$
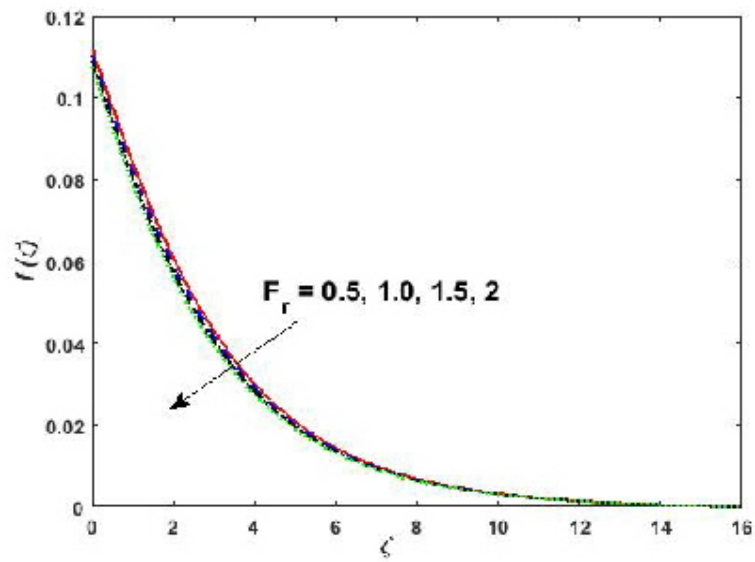
Fig. 3.4 (a) Change in F_r on $f(\zeta)$

38
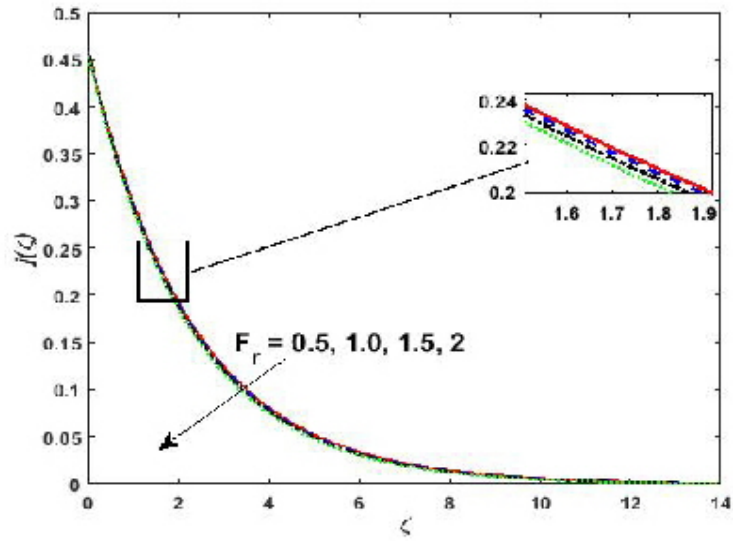
Fig. 3.4 (b) Change in F_r on $j(\zeta)$
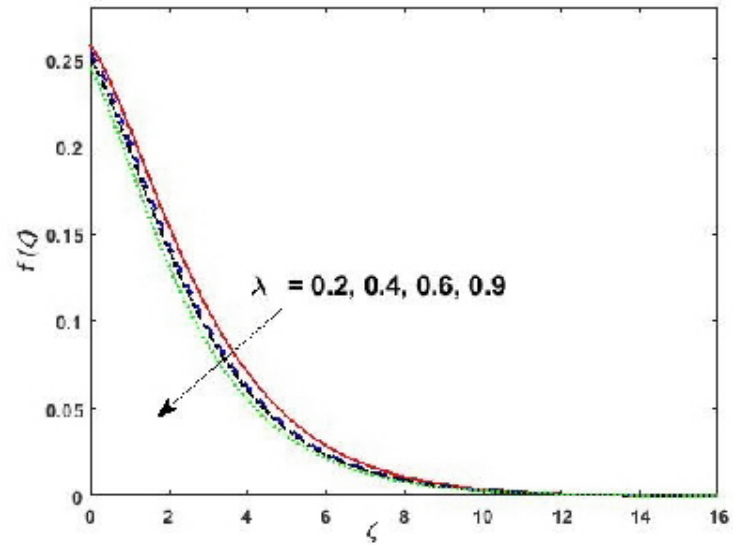
Fig. 3.5 (a) Change in λ on $f(\zeta)$
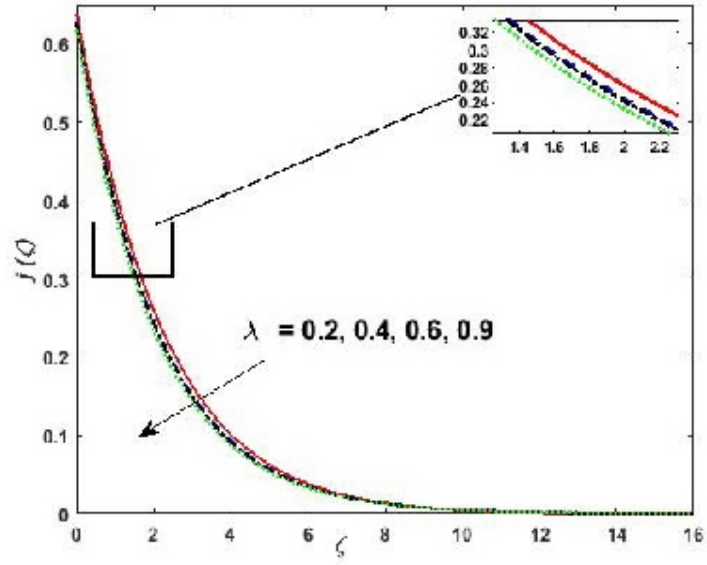
Fig. 3.5 (b) Change in λ on $j(\zeta)$
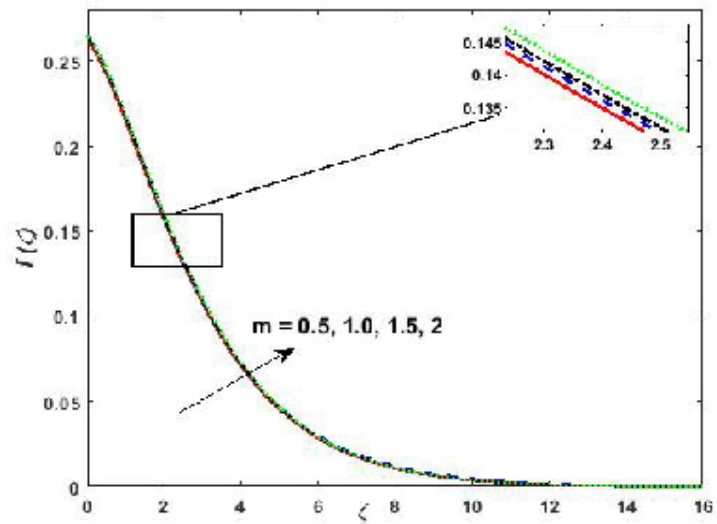
Fig. 3.6 (a) Change in m on $f(\zeta)$
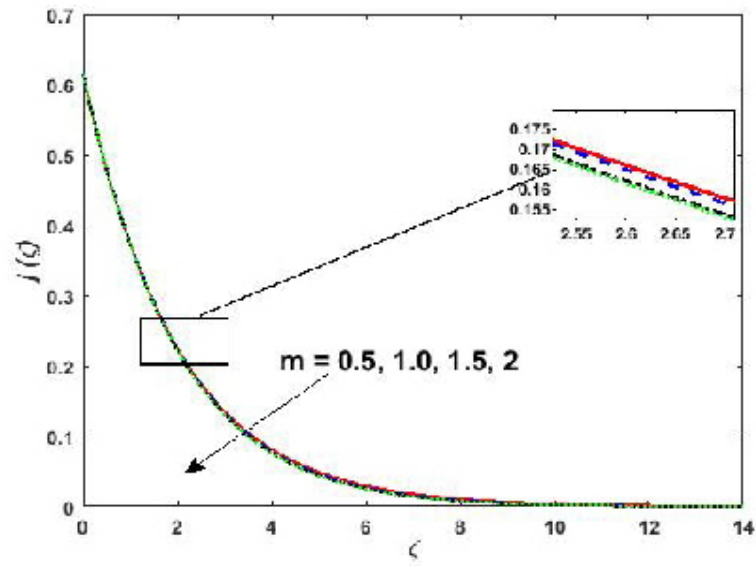
Fig. 3.6 (b) Change in m on $j(\zeta)$
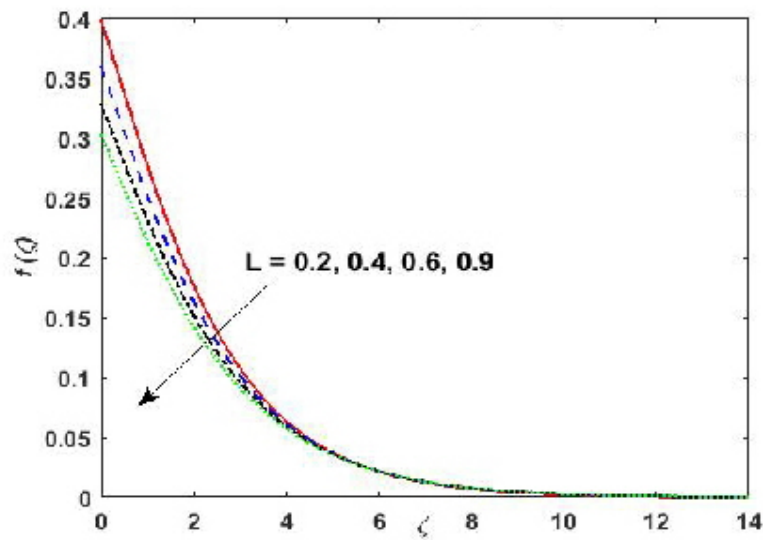
Fig. 3.7 (a) Change in L on $f(\zeta)$

41
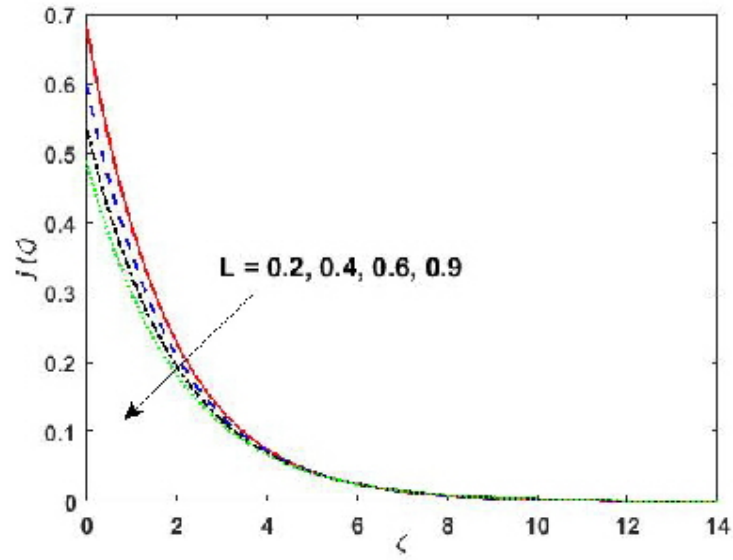
Fig.3.7 (b) Change in L on $j(\zeta)$
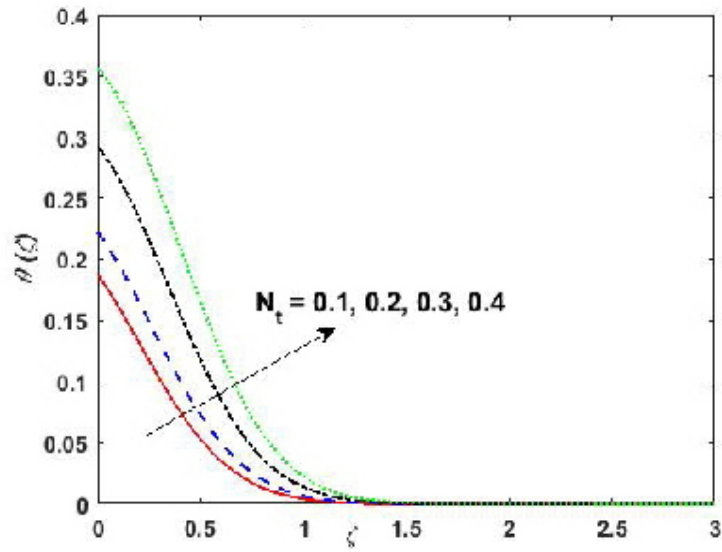
Fig. 3.8 Change in N_t on $\theta(\zeta)$
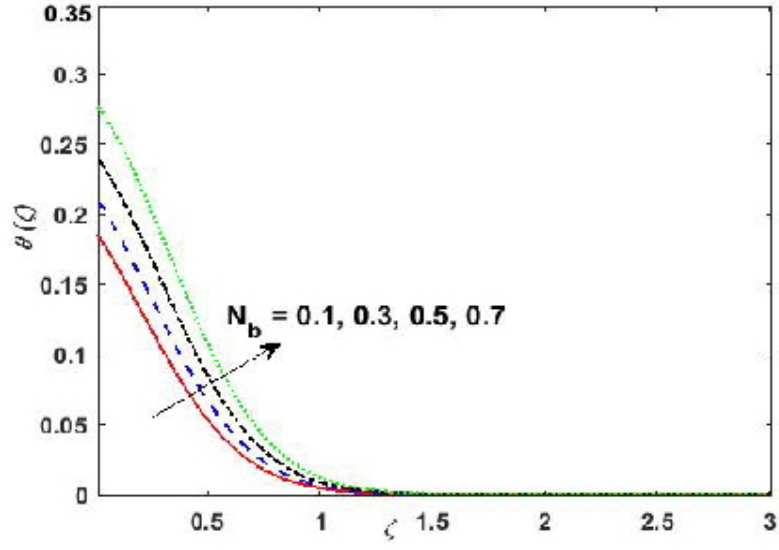
Fig. 3.9 Change in N_b on $\theta(\zeta)$
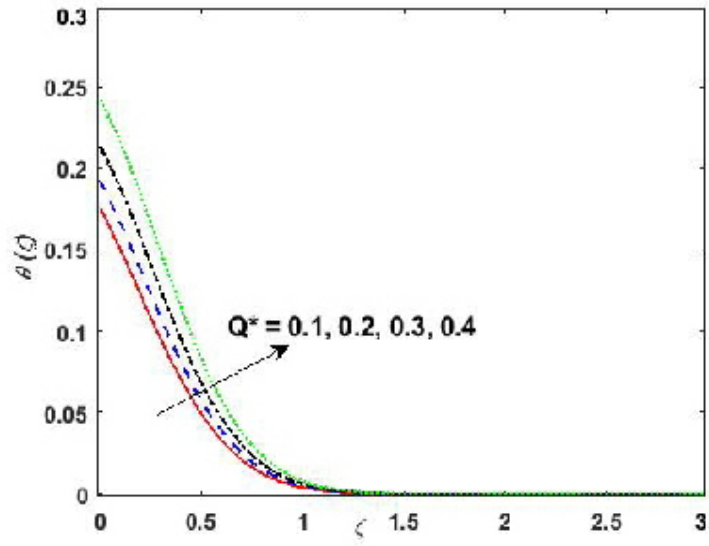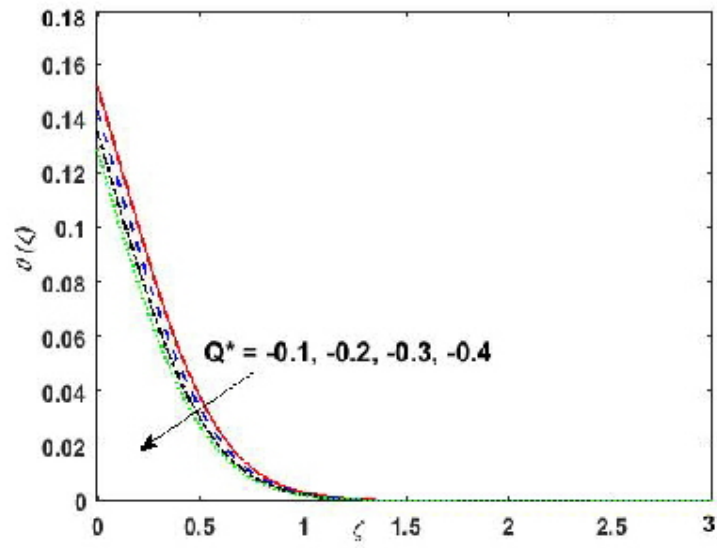

Fig. 3.10 (a) Change in $Q^* > 0$ on $\theta(\zeta)$

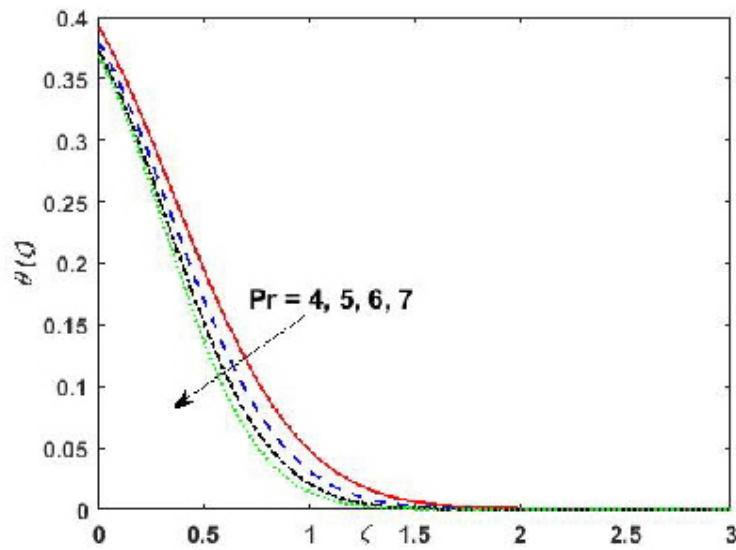Fig. 3.10 (b) Change in $Q^* < 0$ on $\theta(\zeta)$

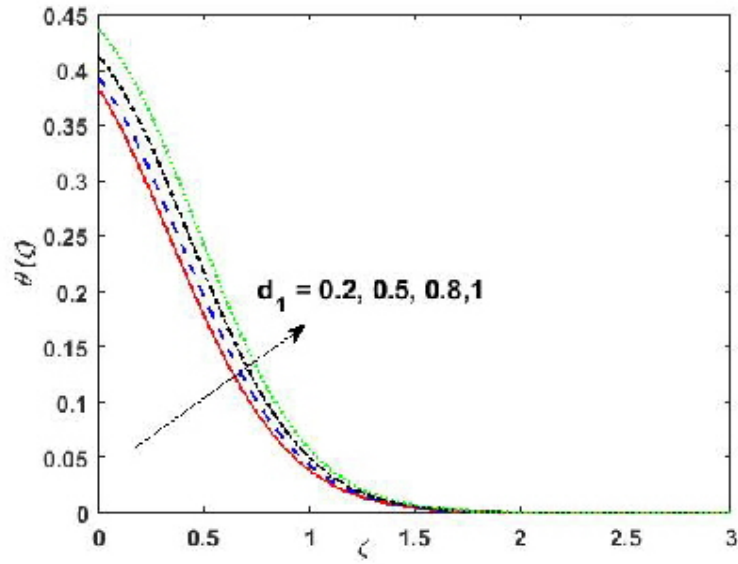Fig. 9.11 Change in P_r on $f(\zeta)$

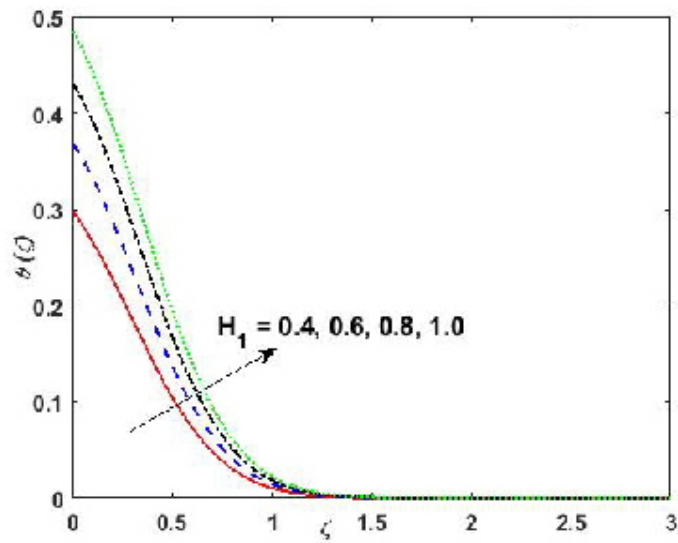Fig. (3.12)   Change in d_1 on $\theta(\zeta)$

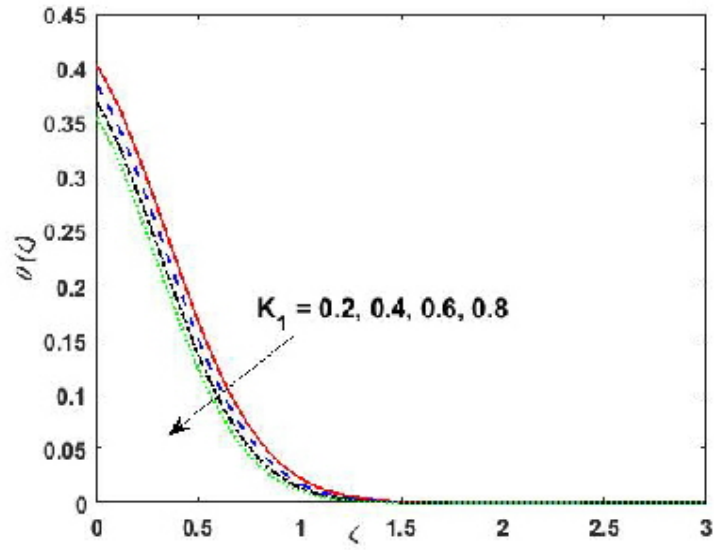Fig. 3.13   Change in H_1 on $\theta(\zeta)$

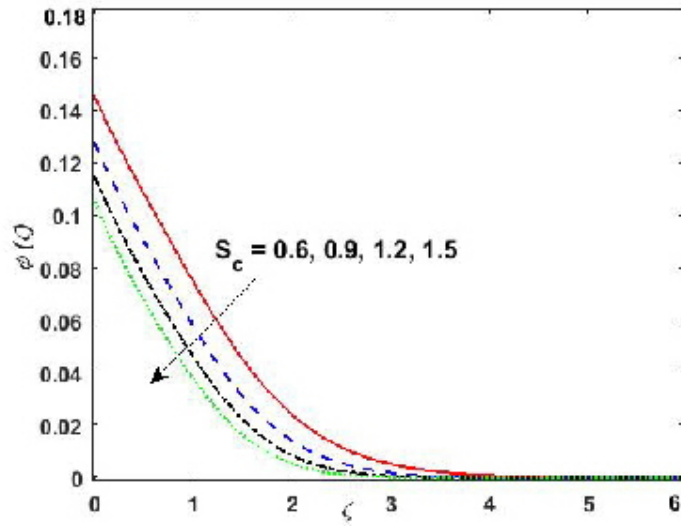Fig. 3.14 Change in K_1 on $\theta(\zeta)$
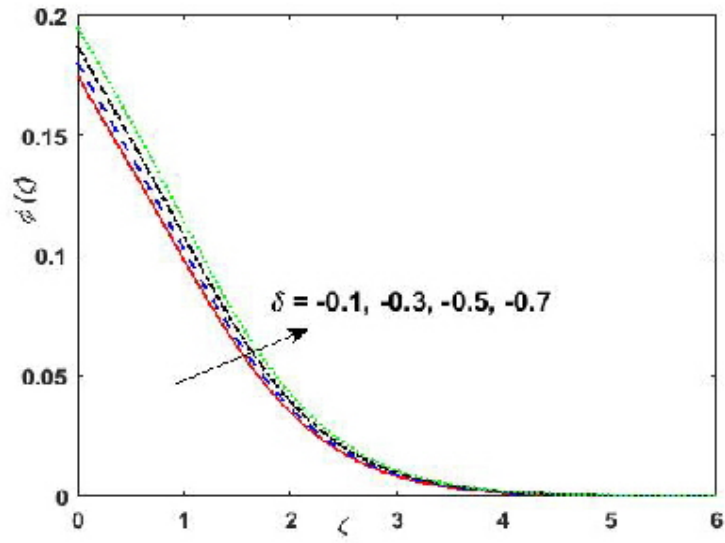

Fig. 3.15 Change in Sc on $\phi(\zeta)$

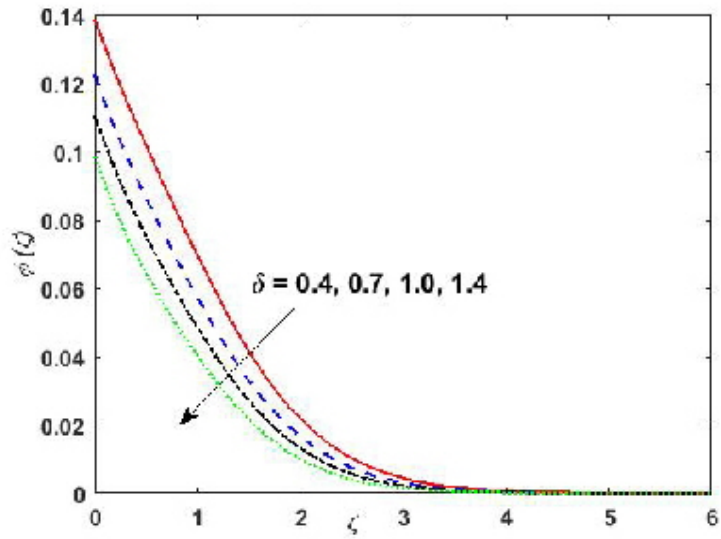Fig. 3.16 (a) Change in $\delta \leq 0$ on $\phi(\zeta)$

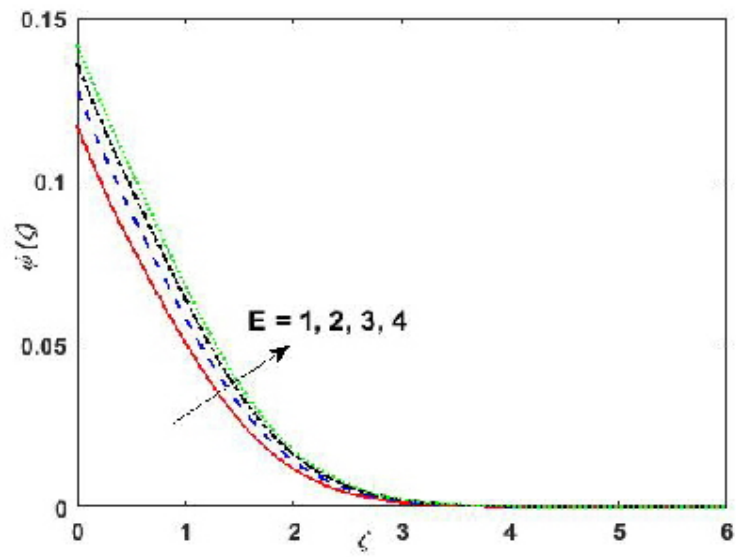Fig. 3.16 (b) Change in $\delta > 0$ on $\phi(\zeta)$
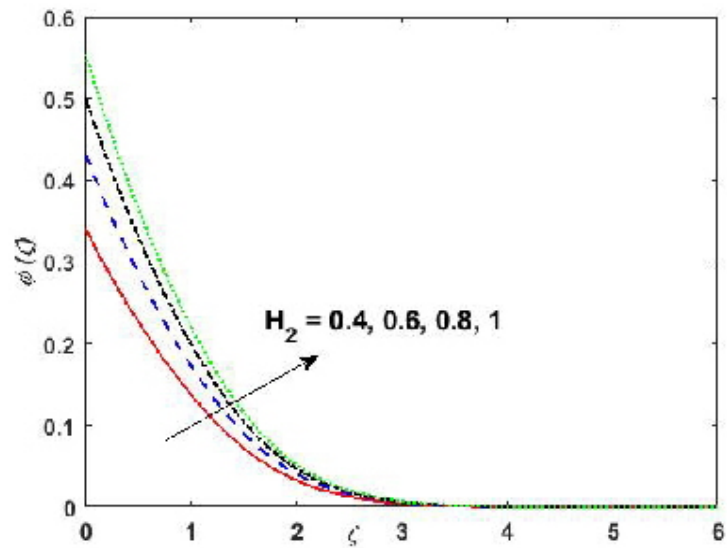
47

Fig. 3.17   Change in E on $\phi(\zeta)$

Fig. 3.18   Change in H_2 on $\phi(\zeta)$

48
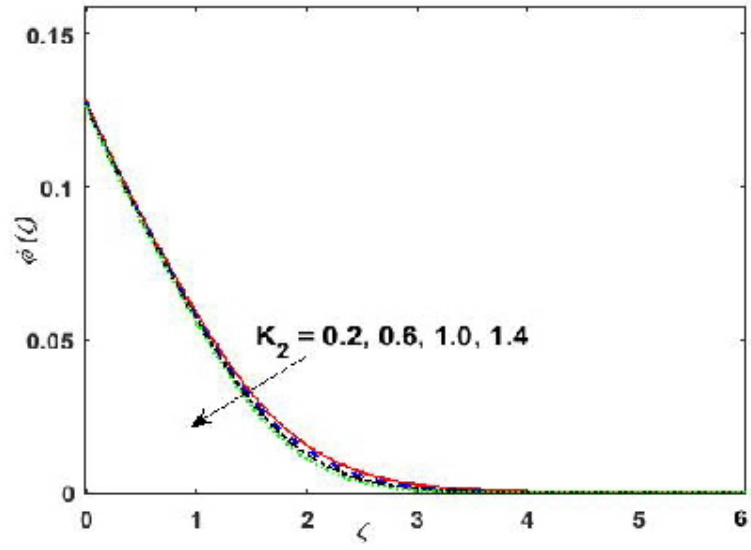
Fig. 3.19 Change in K_2 on $\phi(\zeta)$

Table 3.1: Computational values of fricition drag coefficient $C_f \left(\mathrm{Re}_r\right)^{0.5}$ for different of Ha, P and λ.

p	λ	Ha	$C_f \left(\mathrm{Re}_r\right)^{0.5}$
0.5	0.4	0.5	1.52531
0.8			1.82173
1.1			1.97694
	0.4		1.48810
	0.8		1.53702
	1.2		1.60334
		0.6	1.37931
		0.9	1.50554
		1.2	1.64622

Table 3.2: Computational values of $Nu_r \, \mathrm{Re}_r^{-0.5}$, against different estimation d, H_1, Pr, and N_t.

N_t	d	H_1	P_r	$Nu_r \, \mathrm{Re}_r^{-0.5}$
0.3	0.2	0.5	6.7	0.391959221
0.5				0.26499754
0.7				0.18095062
	0.6			0.36807021
	0.8			0.31930138
	1.2			0.19386025
		0.6		0.48999863
		0.9		0.55012987
		1.1		0.57740485
			4	0.42942989
			5	0.44109717
			6	0.64147684

Table 3.3: Numerical values of for different values of Sc, H_2, E, e and δ.

Sc	e	δ	H_2	E	$Sh_r\,\mathrm{Re}_r^{-0.5}$
0.8	0.1	0.6	0.5	1	0.15184163
1.2					0.22301181
1.4					0.24832378
	0.3				0.06864036
	0.4				0.06686522
	0.5				0.06522742
		1			0.12420382
		1.5			0.17449013
		2			0.21237543
			0.3		0.06905236
			0.6		0.11097549
			0.9		0.13099633
				2	0.04066718
				3	0.02324182
				4	0.01534972

Table 3.4: Validation of $f(0), -j(0)$ and - $\theta(0)$ when $K_1 = Nt = \lambda = Q^* = m = d = Nt = Ha = K_1 = 0$, $\beta \to \infty, Nb \to 0$,$Pr = 6$,with Hafeez et al. [58], Yin et al. [57], and Turkyilmazoglu [56] with the present work

	Hafeez et al. [58]	Yin et al. [57]	Turkyilmazoglu [56]	Present
$f(0)$	0.51011626	0.51022941	0.51023262	0.51026466
$-j'(0)$	0.61584927	0.61591990	0.61592201	0.61594897
$-\theta'(0)$	0.933697411	0.93387285	0.93387794	0.93386285

Chapter 4

SIGNIFICANCE OF HALL CURRENT AND ION SLIP IN A THREE-DIMENSIONAL MAXWELL NANOFLUID FLOW OVER ROTATING DISK WITH VARIABLE CHARACTERISTICS

In this chapter 3D-Maxwell bio-convective nanofluid flow over a rotating deformable disk with variable chracteristics with Hall current and Ion-slip is discussed. The C-C heat flux, mass flux, convective boundary conditions, momentum slip, and bio-convection are all being investigated to understand how they affect mass transfer. The novelty of this model is to enhance the chracteristics of Maxwell fluid with additional effects of Hall current and Ion-slip, bio-convective and veriable chracteristics. Using Von karmann similarities transformation are engaged to convert the partial differential equations into the ordinary differential equations. The bvp4c function in MATLAB provides a numerical solution for a system of differential equations. the numerical results of the mathematical model are represented through graphs

and tables. The endorsement of the stated model is done by comparing it with a previously published article.

4.1 Mathematical Formulation

We assume an incompressible, time-independent 3D-Maxwell bioconvective nanofluid flow over a rotating deformable disk. The disk is centred at $z = 0$ and rotates with a constant angular velocity Ω. The flow of fluid is axisymmetric and takes place on the top plane $z \geq 0$ of a disk that is stretched in the radial direction. The rotation and stretching of a disk causes the fluid to move. The Hall effect and Ion-slip impact on the disk are generally investigated due to the strong magnetic field. Let u, v and w be the velocity components along the directions of growing r, ϕ, and z respectively. The problem geometry in cylindrical coordinates is depicted in Fig. (4.1). The velocity slip, convective boundary conditions and impact of gyrotactic microorganism, are considered here.
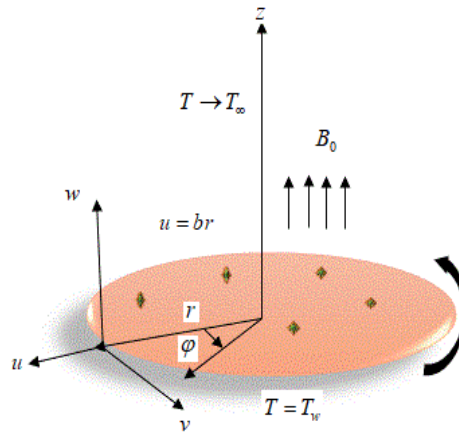

Fig 4.1 Schematic illustration of the flow

$$\frac{\partial u}{\partial r} + \frac{u}{r} + \frac{\partial u}{\partial z} = 0,\qquad(4.1)$$

53

$$u\frac{\partial u}{\partial r} + w\frac{\partial u}{\partial z} - \frac{v^2}{r} + \lambda_0 \left(\begin{array}{c} u^2\frac{\partial^2 u}{\partial r^2} + w^2\frac{\partial^2 u}{\partial z^2} + 2uw\frac{\partial^2 u}{\partial r\partial z} - \frac{2uv}{r}\frac{\partial v}{\partial r} \\ - \frac{2vw}{r}\frac{\partial v}{\partial z} + \frac{uv^2}{r^2} + \frac{v^2}{r}\frac{\partial u}{\partial r} \end{array} \right) =$$
$$\frac{1}{\rho}\frac{\partial}{\partial z}\left(\mu\left(T\right)\frac{\partial u}{\partial z}\right) - \frac{\sigma\beta_o^2}{\rho\left(\left(1+\beta_e.\beta_i\right)^2+\beta_e^2\right)}\left(\begin{array}{c}\left(1+\beta_e.\beta_i\right)u\\ \\ -\beta_e v\end{array}\right), \tag{4.2}$$

$$u\frac{\partial v}{\partial r} + w\frac{\partial v}{\partial z} + \frac{uv}{r} + \lambda_0 \left(\begin{array}{c} u^2\frac{\partial v^2}{\partial r^2} + w^2\frac{\partial v^2}{\partial z^2} + 2uw\frac{\partial^2 v}{\partial r\partial z} + \frac{2uv}{r}\frac{\partial u}{\partial r} + \\ \frac{2vw}{r}\frac{\partial u}{\partial r} - \frac{2u^2v}{r^2} - \frac{v^3}{r^2} + \frac{v^2}{r}\frac{\partial v}{\partial r} \end{array} \right) =$$
$$\frac{1}{\rho}\frac{\partial}{\partial z}\left(\mu\left(T\right)\frac{\partial v}{\partial z}\right) - \frac{\sigma\beta_0^2}{\rho\left(\left(1+\beta_e.\beta_i\right)^2+\beta_e^2\right)}\left(\begin{array}{c}\left(1+\beta_e.\beta_i\right).v\\ \\ +\beta_e.u\end{array}\right), \tag{4.3}$$

$$u\frac{\partial T}{\partial r} + w\frac{\partial T}{\partial z} + \lambda_1 \left(\begin{array}{c} u\frac{\partial T}{\partial r} + 2uw\frac{\partial T}{\partial r\partial z} + w\frac{\partial T}{\partial z} + u\frac{\partial w}{\partial r}\frac{\partial T}{\partial z} \\ +u\frac{\partial u}{\partial r}\frac{\partial T}{\partial r} + w\frac{\partial u}{\partial z}\frac{\partial T}{\partial r} + w\frac{\partial w}{\partial z}\frac{\partial T}{\partial z} \end{array} \right) =$$
$$\frac{1}{\rho C_p}\frac{\partial}{\partial z}\left(K\left(T\right)\frac{\partial T}{\partial z}\right) + \tau\left(\begin{array}{c}D_B\left(\frac{\partial T}{\partial r}\frac{\partial C}{\partial r}+\frac{\partial T}{\partial z}\frac{\partial C}{\partial z}\right)\\ +\frac{D_T}{T_\infty}\left(\left(\frac{\partial T}{\partial r}\right)^2+\left(\frac{\partial T}{\partial z}\right)^2\right)\end{array}\right) - \frac{1}{\rho C_p}Q_1\left(T-T_\infty\right), \tag{4.4}$$

$$u\frac{\partial C}{\partial r} + w\frac{\partial C}{\partial z} + \lambda_2 \left(\begin{array}{c} u^2\frac{\partial^2 c}{\partial r^2} + 2uw\frac{\partial^2 C}{\partial r\partial z} + w^2\frac{\partial^2 C}{\partial z^2} + u\frac{\partial w}{\partial r}\frac{\partial C}{\partial z} + \\ u\frac{\partial u}{\partial r}\frac{\partial C}{\partial r} + w\frac{\partial u}{\partial z}\frac{\partial C}{\partial r} + w\frac{\partial w}{\partial z}\frac{\partial C}{\partial z} \end{array} \right) =$$
$$\frac{\partial}{\partial z}\left(D_B\left(C\right)\frac{\partial C}{\partial z}\right) + \frac{D_T}{T_\infty}\left(\frac{\partial^2 T}{\partial r^2}+\frac{1}{r}\frac{\partial T}{\partial r}+\frac{\partial^2 T}{\partial z^2}\right), \tag{4.5}$$

$$u\frac{\partial N}{\partial r} + w\frac{\partial N}{\partial z} + \frac{bw_e}{\left(C-C_\infty\right)}\left(\frac{\partial N}{\partial z}\frac{\partial C}{\partial z} + N\frac{\partial^2 C}{\partial z^2}\right) = D_n\left(\frac{\partial^2 N}{\partial r^2}+\frac{1}{r}\frac{\partial N}{\partial r}+\frac{\partial^2 N}{\partial z^2}\right). \tag{4.6}$$

with the following boundary conditions:

$$\text{At} \quad z=0 \quad u = br + S\mu\frac{\partial u}{\partial z} \quad ,v = r\Omega + S\mu\frac{\partial v}{\partial z}, \quad w = 0,$$
$$-K\left(T\right)\frac{\partial T}{\partial z} = h_1\left(T_w - T\right), \quad D_B\left(C\right)\frac{\partial C}{\partial z} = h_2\left(C_w - C\right) \quad , \quad N = N_w, \tag{4.7}$$
$$\text{as} \quad z\to\infty \quad u\to 0, \quad v\to 0, \quad T\to T_\infty, \quad C\to C_\infty, \quad N\to N_\infty.$$

$\mu\left(T\right)$ the (variable viscosity), that is(temperature dependent) and denoted by [60]:

$$\mu\left(T\right) = \frac{\mu_\infty}{\left(1+\left(T-T_\infty\right).\lambda_3\right)}. \tag{4.8}$$

The free stream viscosity is represented by μ_∞. The consideration of viscosity for heat changes is classified by the value of. As for $0 > \lambda_3$, it denotes gaseous fluids, whereas $\lambda_3 > 0$ denotes liquid fluids. $\lambda_3 = 0$ for Newtonian fluid

The variable thermal conductivity varies with temperature is given by

$$K(T) = K_\infty \left[1 + d \left(\frac{T - T_\infty}{T_w - T_\infty} \right) \right]. \tag{4.9}$$

The variable molecule diffusivity is given as

$$D_B(C) = K_\infty \left[1 + e \left(\frac{C - C_\infty}{C_w - C_\infty} \right) \right]. \tag{4.10}$$

Using appropriate transformations:

$$u = r\Omega f(\eta), \quad v = r\Omega g(\eta), \quad w = (\Omega v)^{\frac{1}{2}} h(\eta), \quad \theta(\eta) = \frac{T - T_w}{T_w - T_\infty},$$

$$\phi(\eta) = \frac{C - C_w}{C_w - C_\infty}, \quad \xi(\eta) = \frac{N - N_\infty}{N_w - N_\infty}, \quad \eta = \left(\frac{\Omega}{v} \right)^{\frac{1}{2}} Z. \tag{4.11}$$

Eqs. $(4.1) - (4.6)$ become:

$$h'(\eta) + 2f = 0, \tag{4.12}$$

$$\left[\begin{array}{c} \left(\dfrac{1}{1 + \lambda^* \theta(\eta)} - \beta_1 (h(\eta))^2 \right) f''(\eta) - \dfrac{\lambda^* . \theta'(\eta) f'(\eta)}{(1 + \lambda^* \theta(\eta))^2} \\[2mm] - \left(f^2(\eta) + f(\eta) h(\eta) - g(\eta) \right) - \\[2mm] \beta_1 \left(\begin{array}{c} 2f(\eta) f'(\eta) - 2g(\eta) f(\eta) \\[1mm] -2h(\eta) g(\eta) g'(\eta) + g^2(\eta) f(\eta) + g(\eta) f(\eta) \end{array} \right) - \\[2mm] \left(\dfrac{M}{(1 + \beta_e . \beta_i)^2 + B_e^2} \right) \left((1 + \beta_e . \beta_i) . f(\eta) - B_e . g(\eta) \right) \end{array} \right] = 0, \tag{4.13}$$

$$\left[\begin{array}{l} \left(\dfrac{1}{1+\lambda^*\theta\left(\eta\right)}-\beta_1 h\right)g''\left(\eta\right)-\dfrac{\lambda^*.\theta'\left(\eta\right)g'\left(\eta\right)}{\left(1+\lambda^*\theta\left(\eta\right)\right)^2}-\left(\begin{array}{l}2g\left(\eta\right)f\left(\eta\right)+\\ h\left(\eta\right)g'\left(\eta\right)\end{array}\right) \\ \qquad -\beta_1\left(\begin{array}{l}2f\left(\eta\right)g\left(\eta\right)h\left(\eta\right)+2g\left(\eta\right)f'\left(\eta\right)+\\ 2f'\left(\eta\right)g\left(\eta\right)h\left(\eta\right)+2g\left(\eta\right)f^2\left(\eta\right)\end{array}\right) \\ \qquad -\dfrac{M}{\left(\left(1+\beta_e.\beta_i\right)^2+B_e^2\right)}\left(\left(1+\beta_e.\beta_i\right).g\left(\eta\right)+B_e.f\left(\eta\right)\right). \end{array}\right]=0, \qquad (4.14)$$

$$\left[\begin{array}{l} \left(\begin{array}{l}\left(1+d_1\theta\left(\eta\right)\right)\\ -\Pr k_1 h^2\left(\eta\right)\end{array}\right)\theta''\left(\eta\right)+d_1\left(\theta'\left(\eta\right)\right)^2+ \\ \Pr\left(\begin{array}{l}N_b\theta'\left(\eta\right)\phi\left(\eta\right)+N_t\left(\theta'\left(\eta\right)\right)^2-h\left(\eta\right)\theta'\left(\eta\right)\\ -k_1 h\left(\eta\right)h'\left(\eta\right)\theta'\left(\eta\right)+Q^*\theta\left(\eta\right)\end{array}\right) \end{array}\right]=0, \qquad (4.15)$$

$$\left[\begin{array}{l} \left(\left(1+e\phi\left(\eta\right)\right)-K_2.S_c.h^2\left(\eta\right)\right)\phi''\left(\eta\right)+e\left(\phi'\left(\eta\right)\right)^2 \\ +N_t\dfrac{1}{N_b}\theta''\left(\eta\right)-S_c\left(h\left(\eta\right).\phi'\left(\eta\right)+k_2.h\left(\eta\right)h'\left(\eta\right)\theta'\left(\eta\right)\right) \end{array}\right]=0, \qquad (4.16)$$

$$\xi''\left(\eta\right)-\left(Lbf'\left(\eta\right)+pe\xi'\left(\eta\right)\theta\left(\eta\right)+pe\left[\Omega+\xi\left(\eta\right)\phi''\left(\eta\right)\right]\right)=0. \qquad (4.17)$$

Dimensionless boundary conditions are

$$\begin{array}{llll} At \quad \eta \;=\; 0\,, & f\left(0\right)=P+Lf'\left(\eta\right), & g\left(0\right)=1+Lg\left(\eta\right), & h\left(0\right)=0, \\[4pt] \theta\left(\eta\right) \;=\; -H_1\left(\dfrac{1-\theta\left(0\right)}{1+d\theta}\right), & \phi\left(\eta\right)=-H_2\left(\dfrac{1-\phi\left(0\right)}{1+e\phi}\right), & \xi\left(0\right)=1, \\[8pt] As \quad \eta \;\to\; \infty\,, & f\to 0, \quad g\to 0, & \theta\to 0, \quad \phi\to 0, & \xi\to 0. \quad (4.18) \end{array}$$

The expression for dimensionless parameter given in equation $(4.12)-(4.18)$ are

$$\begin{array}{l} \Pr=\dfrac{\mu c_p}{k_\infty},N_b=\dfrac{\tau D_B\left(C_w-C_\infty\right)}{v},N_b=\dfrac{\tau D_T\left(T_w-T_\infty\right)}{vT_\infty},L=S\mu\sqrt{\dfrac{\Omega}{v}}.K_1=\lambda_1\Omega, \\[6pt] K_2=\lambda_2\Omega,H_1=\dfrac{h_1}{k_\infty}\sqrt{\dfrac{v}{\Omega}},H_2=\dfrac{h_2}{k_\infty}\sqrt{\dfrac{v}{\Omega}},Q^*=\dfrac{Q_1}{\rho c_p\Omega},\beta_1=\lambda_0\Omega,M=\dfrac{\sigma B_0^2}{\rho\Omega},. \\[6pt] P=\dfrac{b}{\Omega},\mathrm{Re}=\dfrac{\Omega}{v}r^2,Le=\dfrac{v}{D_m},Pe=\dfrac{bw_e}{D_m},\Omega=\dfrac{N_\infty}{N_w-N_\infty}. \end{array} \qquad (4.19)$$

where $\lambda^*,\beta_1,Nt,H_2,,Sc,\;Nb\,,e,k_1,H_1,k_2,P,L,\beta_i,M,\Pr,d_1,Q^*,\beta_e,Lb,Pe,$ are represents the viscosity with respect to temperature, Deborah number, Thermophoresis parameter, variable thermal conductivity, Mass transfer, Biot number, Schmidt number, Brownian motion parame-

ter, variable molecular diffussivity, thermal relaxation   parameter, Lewis number, heat transfer Biot number, concentration relaxation parameter, stretching parameter, velocity slip parameter, ion-slip parameter, magnetic parameter, Prandtl number, heat source parameter to the angular velocity, hall current parameter, Peclet number respectively.

The wall shear stress (drag force coefficient), heat transfer rate Nu_r, and mass transfer Sh_r, are defined as follows:

$$C_f = \frac{\tau_w}{\rho\,(\Omega r)^2}, \quad \text{where} \quad \tau_w = \left(\tau_{zr}^2 + \tau_{z\theta}^2\right)^{\frac{1}{2}},$$

$$\text{where} \quad \tau = \mu\frac{\partial u}{\partial z}|_{z=0}, \quad \tau_{z\theta} = \mu\frac{\partial v}{\partial z}|_{z=0}, \tag{4.20}$$

$$Nu_r = \frac{rQ_w}{K_\infty\,(T - T_\infty)}, \quad \text{where} \quad Q_w = -K(T)\frac{\partial T}{\partial z}|_{z=0}, \tag{4.21}$$

$$Sh_r = \frac{rQ_m}{D_B\,(C - C_\infty)}, \quad Q_m = -D_B\frac{\partial C}{\partial z}|_{z=0}. \tag{4.22}$$

By utillizing Eqs. (4.11) Eqs. (4.20) − (4.22) are transmuted as:

$$C_f\,\mathrm{Re}_r^{0.5} = \left[f\,'(\eta)^2 + \left(g'(\eta)\right)^2\right]^{\frac{1}{2}}|_{\eta=0}, \tag{4.23}$$

$$Nu_r\,\mathrm{Re}_r^{-0.5} = -\left[1 + d_1\theta\,(\eta)\right]\theta'(\eta)\,|_{\eta=0}, \tag{4.24}$$

$$Sh_r\,\mathrm{Re}_r^{-0.5} = -\left[1 + e\phi\,(\eta)\right]\phi'(\eta)\,|_{\eta=0}.$$

4.2   Numerical procedure

The coupled nonlinear Ordinary differential equations (ODEs) are numerically calculated using MATLAB bvp4c function. Higher-order differential equations are reduced to first-order equations. With a tolerance of 10^{-6}, a step size of $h = 0.01$ is is used. The converssion of higher order ODE into ODE of oder one is given as under:

$$f(\eta) = y_1, f'(\eta) = y_2, f''(\eta) = yy_1,$$

$$g(\eta) = y_3, g'(\eta) = y_4, g''(\eta) = yy_2, h(\eta) = y_5, h'(\eta) = yy_3. \tag{4.26}$$

Using Eqs. (4.26) in Eqs. (4.12) − (4.14)

$$
\begin{aligned}
\left(\frac{1}{(1+\lambda^*Y_6)} - \beta_1 (y_5)^2\right) yy_1 &= -\frac{\lambda^*.y_2.y_7}{(1+\lambda^*Y_6)^2} \\
&+ \left((y_1)^2 + y_1 y_5 - (y_3)^2\right) - \\
&\left(\frac{M}{(1-\beta_e.\beta_i)^2 + Be^2}\right)((1-\beta_e.\beta_i).Y_1 - Bey_3) \\
&+\beta_1 \left(2.y_1.y_2. - 2y_2.(y_3)^2 - 2y_3 y_4 y_5 + y_1 (y_3)^2 + y_3 y_1\right),
\end{aligned}
\tag{4.27}
$$

$$
\begin{aligned}
\left[\frac{1}{(1+\lambda^*Y_6)} - \beta_1 y_5\right] yy_2 &= -\frac{\lambda^*.y_4.y_6}{(1+\lambda^* y_6)^2} \\
+ (2y_3 y_1 + y_4 y_5) - \left(\frac{M}{(1-\beta_e.\beta_i)^2 + B_e^2}\right)&((1-\beta_e.\beta_i).y_3 + B_e y_1) \\
+\beta_1 \left(2.y_1.y_4.y_5 + 2y_2.y_3 + 2.y_2.y_3.y_5 + y_3.(y_1)^2 + y_1.y_3\right),
\end{aligned}
\tag{4.28}
$$

$$yy_3 = -2.y_1, \tag{4.29}$$

$$\theta(\eta) = y_6, \theta'(\eta) = y_7, \theta''(\eta) = yy_4, \phi(\eta) = y_8,$$

$$\phi'(\eta) = y_9, \phi''(\eta) = yy_5, \xi(\eta) = y_{10}, \xi'(\eta) = y_{11}, \xi''(\eta) = yy_6. \tag{4.30}$$

Using Eqs. (4.30) is in Eqs. (4.15) - (4.17)

$$\left((1+d_1 y_6) - K.\Pr.(y_5)^2\right) yy_4 = -d_1 (y_7)^2 - \Pr\left(\begin{array}{c} N_b.y_7.y_9 + N_t.(y_7)^2 + \\ Q^*.Y_6 - Y_5.Y_7 - K_1.Y_5.Y_7.yy_3 \end{array}\right), \tag{4.31}$$

$$\left((1+e.Y_8) - K_2.Sc.(Y_5)^2\right) YY_5 = -e.(Y_7)^2 - \left(\frac{Nt}{N_b}\right).YY_4 + Sc\left(\begin{array}{c} Y_5.Y_9 + \\ K_2 Y_3.Y_5.YY_3 \end{array}\right), \tag{4.32}$$

$$YY_6 = Lb.Y_2 + Pe.Y_9.Y_{11} + Pe\left(\Omega + Y_{10}\right)YY_5. \tag{4.33}$$

4.3 Discussion of the findings

The effects of non-dimensional parameters against included profiles in a highly nonlinear mathematical model is graphically investigated. Figs. $4.2 - 4.15$ show that of relevant factors on the velocity field in the radial $f(\eta)$, tangential field $g(\eta)$, and axial field $h(\eta)$. Figs. $3.3a$ and $3.3b$ show the effects of the Deborah number β_1 on $f(\eta)$ and $g(\eta)$. The velocity profile declined for greater value of β_1. because for larger values of β_1, the large value of relaxation time in the fluid implies that the fluid has become more solid-like, that why velocitys profiles decreases $f(\eta)$ and $g(\eta)$. The radial velocity profile $f(\eta)$ for the parameter λ^* is depicted in Fig. 4.4. The decrease in amplitude is due to fact that the boundary layer is decrementing as the profile approaches the disk. Physically rising values of $\lambda^* > 0$ for an isothermally heated disk, causing the fluid around the disk to become low viscous. A decline in the viscous interaction between the fluid and the disk surface, as well shear stress, causes the fluid region of the disk to flow in the radial direction, the result is decrease in the radial profile. Fig. 4.5 depict the effect of λ^* on the velocity profile $g(\eta)$. The azimuthal velocity profile $g(\eta)$ decreases as λ^* is estimated more accurately. Near the disk, the velocity profile decreases. Figs. 4.6-4.7 and 4.8 display the effect of the magnetic filed parameter M on $f(\eta)$, $g(\eta)$, and $h(\eta)$. It is obserued than for higher estimatios of M the radial velocity $f(\eta)$ and tangential velocity $g(\eta)$ are decrecsing. Because Lorentz force is stronger. which causes restance to fluid.The axial velocity $h(\eta)$, on the other hand, show a reversal of the trends when the Hartmann parameter is increased. Figs. $4.9 - 4.10$ show $f(\eta)$ and $g(\eta)$ respond to changes in the ion-slip parameter (β_i). It is visible from Figs. $4.9 - 4.10$ that increasing the β_i leads to reduced in the radial velocity $f(\eta)$ and tangential velocity $g(\eta)$ are increased. In physically, the impact of the Hall parameter β_e on the flow and thermal field is greater than the effect of the β_i.This is due to the fact that electron diffusion velocity is much faster than ion diffusion velocity. Figs. $4.11 - 4.12$ represents the behaviour of Hall's current strategic (β_e) on $f(\eta)$ and $g(\eta)$. The magnetic dampening force's effect is decreased. It has been observed that when the value of β_e increased, leads to a

velocity profile $f(\eta)$ is increased, and velocity profile $g(\eta)$ decreased. The effect of such slip parameter L on $f(\eta)$ and $g(\eta)$ is depicted in Figs. $4.13 - 4.14$. It is observed that when the value of L increases, the friction force increases. As a result, more liquid passes through the deformable revolving disk. That is why, the fluid will flow in $f(\eta)$ and $g(\eta)$ depreciate.The effect of streching parameter P on $f(\zeta)$ is depicted in Figs. 4.15. It has been observed that when the value of P increases, the velociy profile increases. Fig. 4.16 shows the effect of the thermophoresis parameter N_t on $\theta(\eta)$. The thermophoretic force of nanoparticles is intensified by increasing N_t and nanoparticles travel from hot to cool fluid. As a result, $\theta(\eta)$ improves. The effect of the Brownian motion variable N_b on $\theta(\eta)$ is shown in Fig. 4.17. Because the collision of the nanoparticles increases as the value of N_b increases, additional heat is created. It is concluded that $\theta(\xi)$ increases as N_b increases. The impact of heat production and absorption parameter Q^* on $\theta(\eta)$ is seen in Fig. 4.18. It is observed that when Q^* is agumented, a large amount of heat is produced. As a result, the system gains more heat. So, the thermal profile expands, for negtive Q^* it shows oppsitive behavior. As a result, the thermal field decreases. The impact of the Prandtl number P_r on $\theta(\eta)$ is seen in Fig. 19. Since by increasing P_r, the fluid's viscosity increases, while heat diffusion decreases. As a result, heat dissipation from the heated surface decreases. Fig. 4.20 shows the increasing effect for different value of d on $\theta(\eta)$. As the value of d increases, the collision between the nano particles becomes more intense, and more heat is transferred through the fluid. Fig. 4.21 reveal the effect of Biot number (H_1) on $\theta(\eta)$. For increasing values of H_1 heat transfer coefficient improves. It is understood that $\theta(\eta)$ intensifies rapidly for increasing H_1. In Fig. 4.22, the effect of changing Schmidt number Sc on the concentration field $\phi((\eta))$ is explained. It has been noticed that when Sc increases, the Brownian motion parameter decreases and the fluid's concentration is decreased. The thickness of the boundery layer has decreased. Fig. 4.23 reveal the effect of mass transfer Biot number (H_2) on $\phi((\eta))$. For increasing values of H_2 mass transfer coefficient improves. It is understood that $\phi(\eta)$ intensifies rapidly for increasing H_2. In Fig. 3.24, the effect of increasing the concentration relaxation parameter K_2 on $\phi(\eta)$ is shown.It has been shown that when K_2 increases, more time is required for particles diffusion. As a result, increased K_2. Heating causes the system to become more uneven and accelerates the formation of bioconvection. Figs. 4.25 $- 4.26$ show the effect of bioconvection Lewis number (Lb) and Peclet number (Pe) on fluid

motile density. For large values of the Pe, the motile density profile is shown to decline. Fluid motile density decreases with increasing Pe owing to a reduction in microorganism diffusivity. It has also been shown that growing estimates of Lb produce microorganism falloffs, and so the profile of motile density increases in this case. Table 3.1 shows the effect of calculated values of non - dimensional parameters , $\lambda^*, \beta_1, \beta_{i,} \beta_e$ and m on the skin friction coefficient Cf $\mathrm{Re}_r^{0.5}$. shows an ascending profile for higher values of parameters β_e and whereas shows a descending trend for higher value of and parameters$\lambda^*, \beta_1, \beta_{i,}$ and m. Table 4.2 represents the effect of $Nt, K_1, H_1, Q^*, \mathrm{Pr}, N_b,$ and d on the local Nusselt number.The rate of heat transmission is thought to be increasing as Nt, Q^*, Pr ,and H_1 values increase.$Nu_r Re_r^{0.5}$, on the other hand, decreases at increasing values of N_b, K_1 and d. Table 4.3 shown the effect of various $Sc, k_2, H_2,$ and e values on the local Sherwood number.The rate of mass transfer increases as the value of Sc, k_2 and H_2 increase; however, when e increase, the nature of the transfer deteriorates. Table 3.4 shows a comparison of the current work with Turkyilmazoglu [56], Yin et al. [57], Hafeezetal.[58]. and Shaheen, et al [59]. there is a strong correlation between the outcomes.
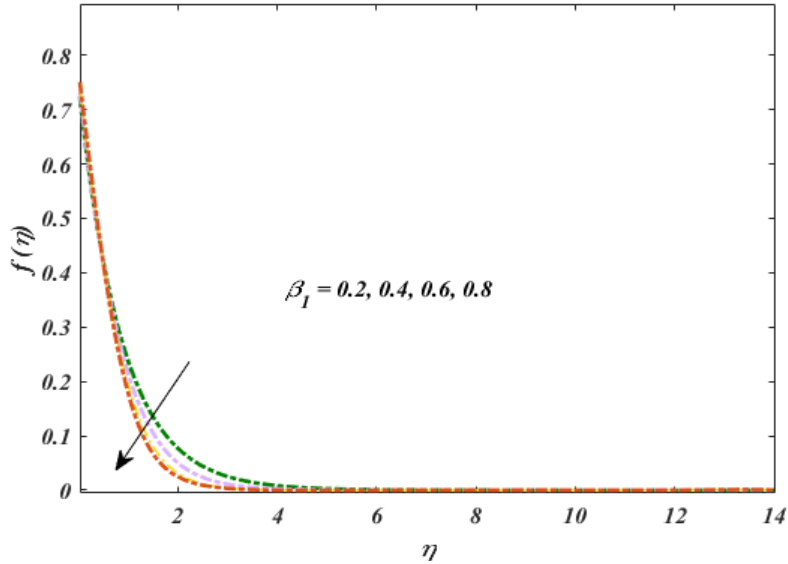
Fig. 4.2 change in $f(\eta)$ vs β_1
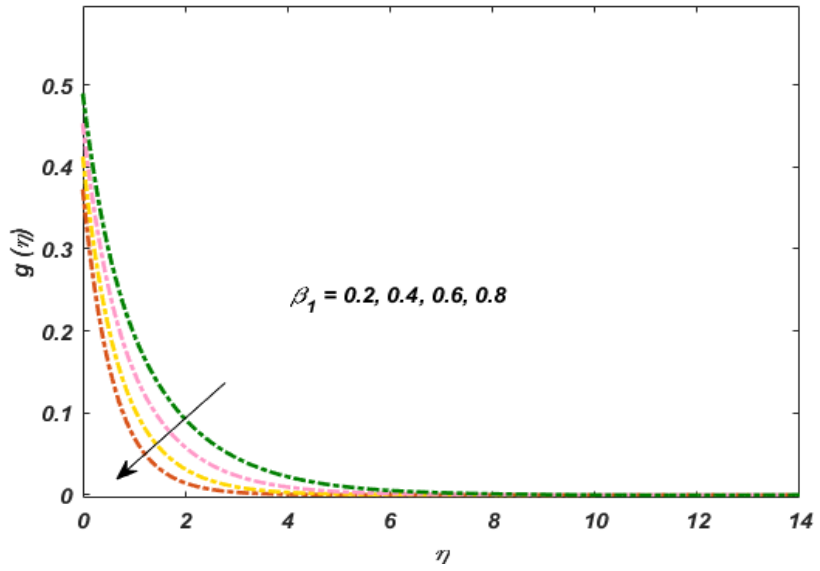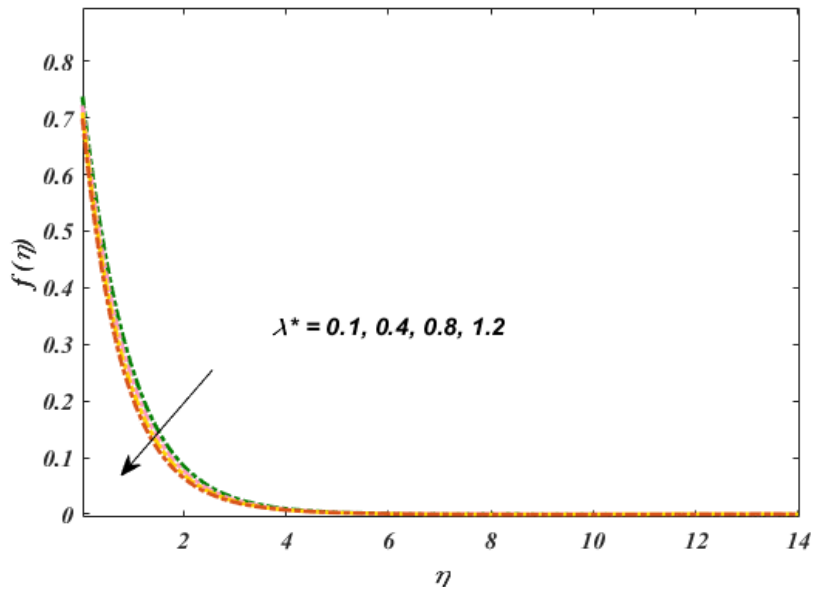
Fig. 4.3 change in $g(\eta)$ vs β_1

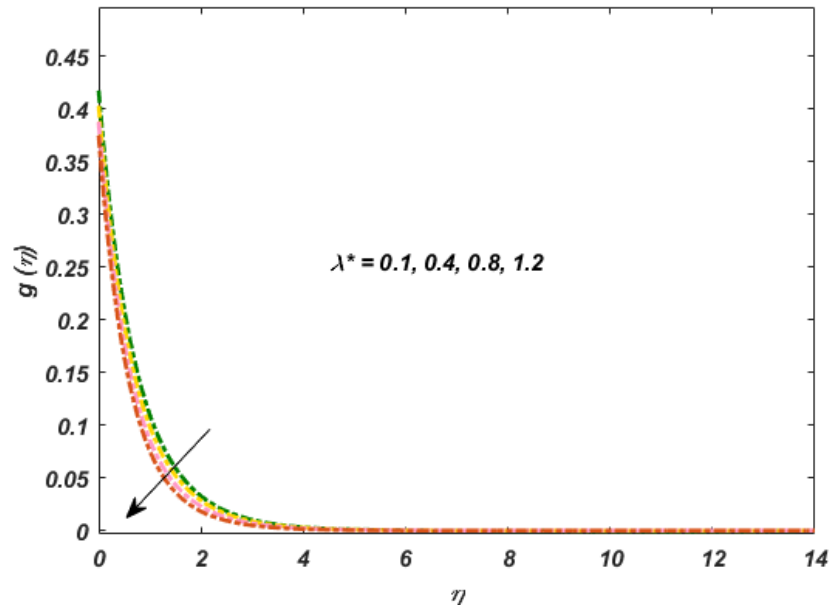Fig. 4.4 change in $f(\eta)$ vs λ^*

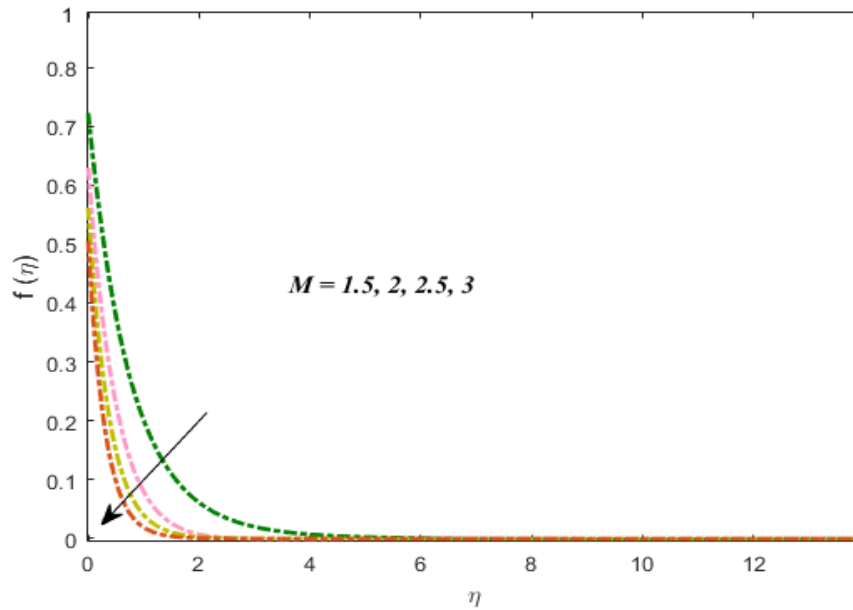Fig. 4.5 change in $g(\eta)$ vs λ^*

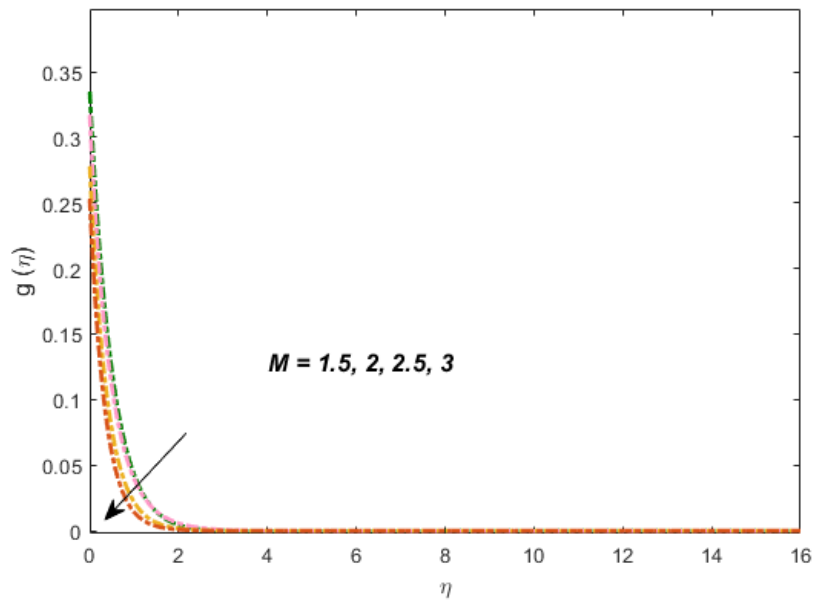Fig. 4.6 change in $f(\eta)$ vs M
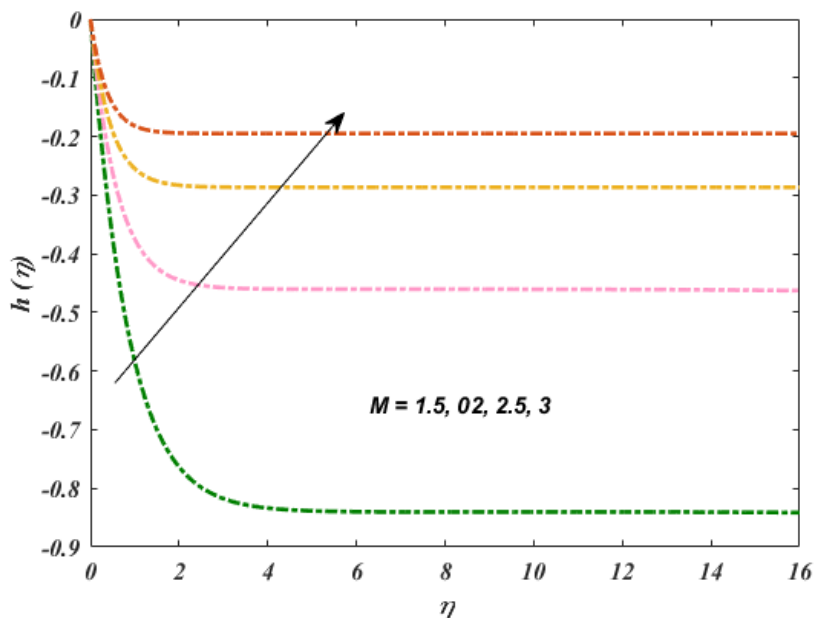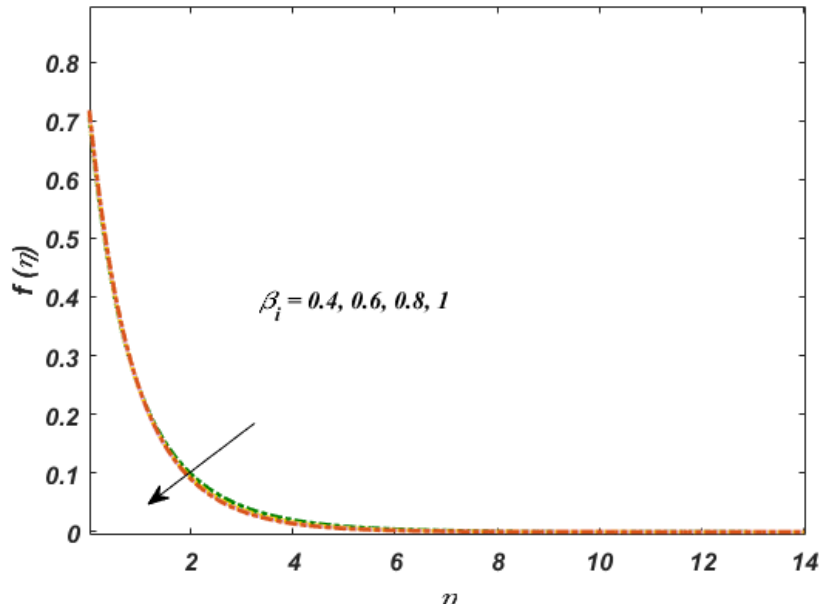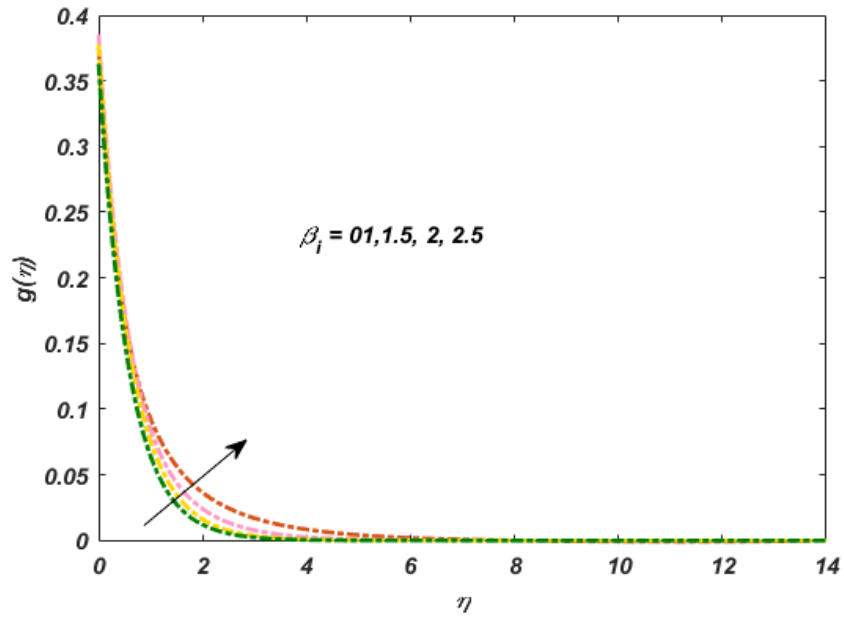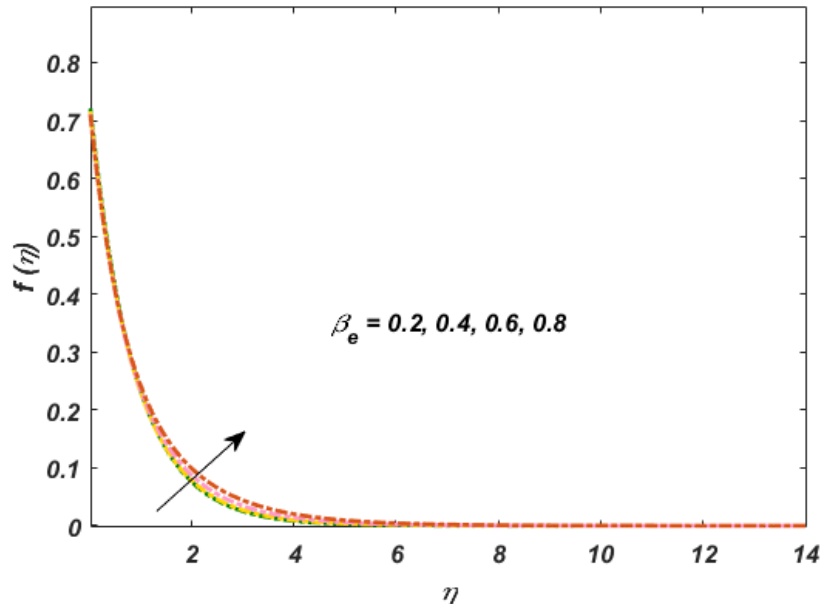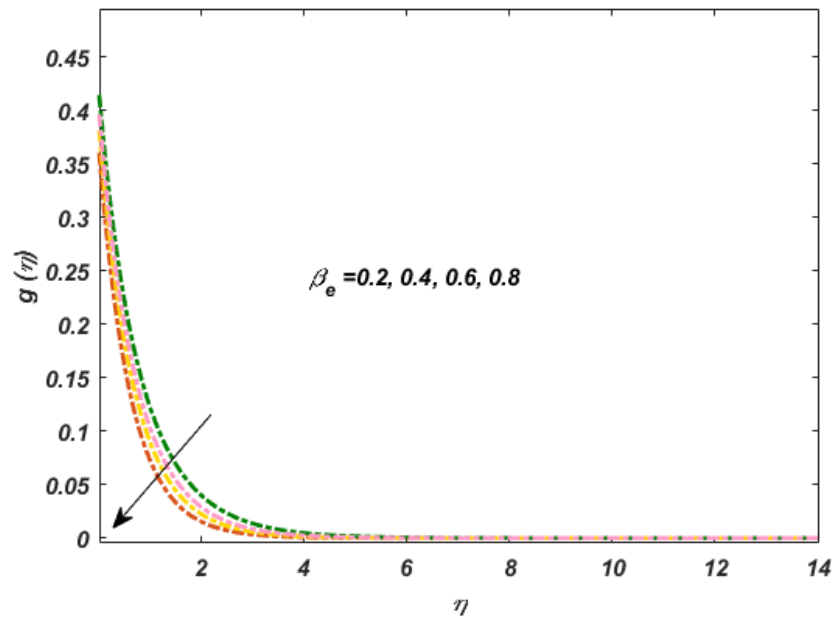
Fig. 4.7 change in $g(\eta)$ vs M

Fig. 4.8 change in $h(\eta)$ vs M

64

Fig. 4.9 change in $f(\eta)$ vs β_i

Fig. 4.10 change in $g(\eta)$ vs β_i

65

Fig. 4.11 change in $f(\eta)$ vs β_e

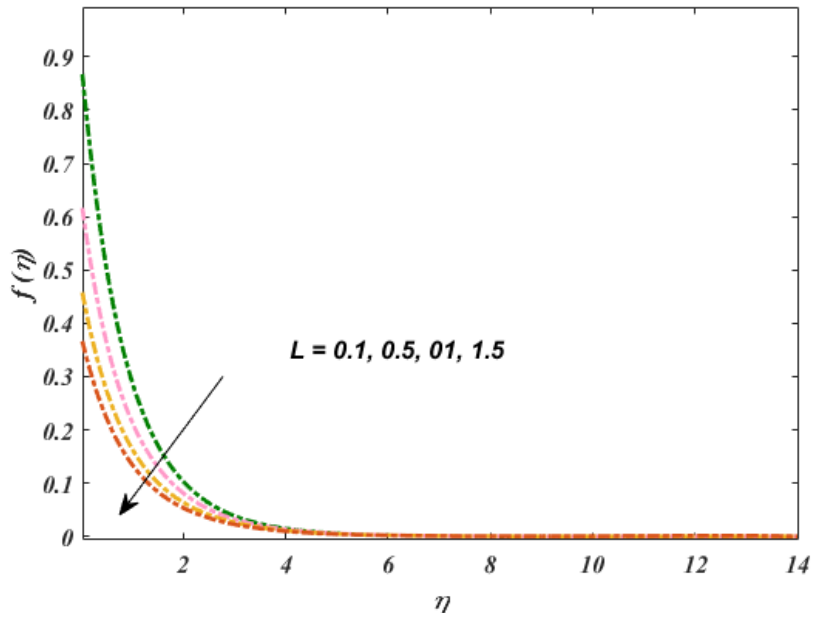Fig. 4.12 change in $g(\eta)/$vs β_e

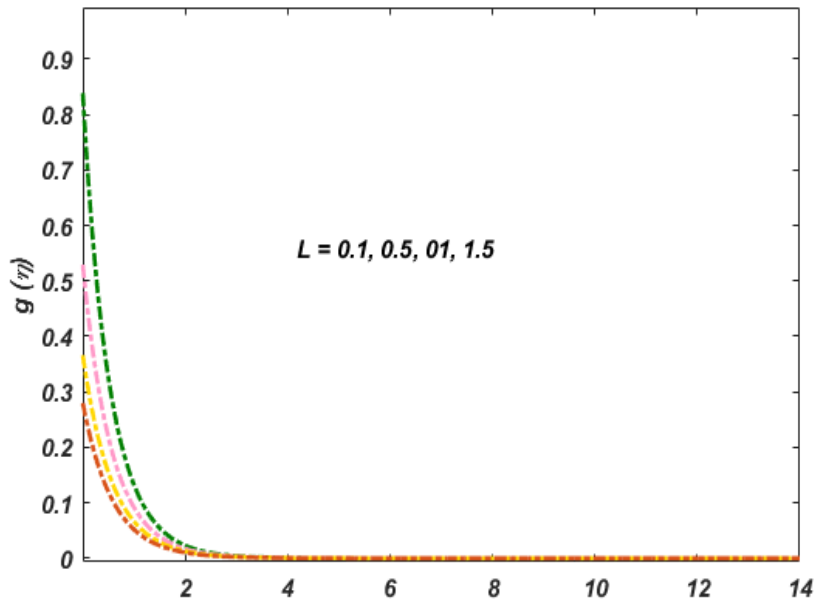Fig. 4.13 Change in $f(\eta)$ vs L

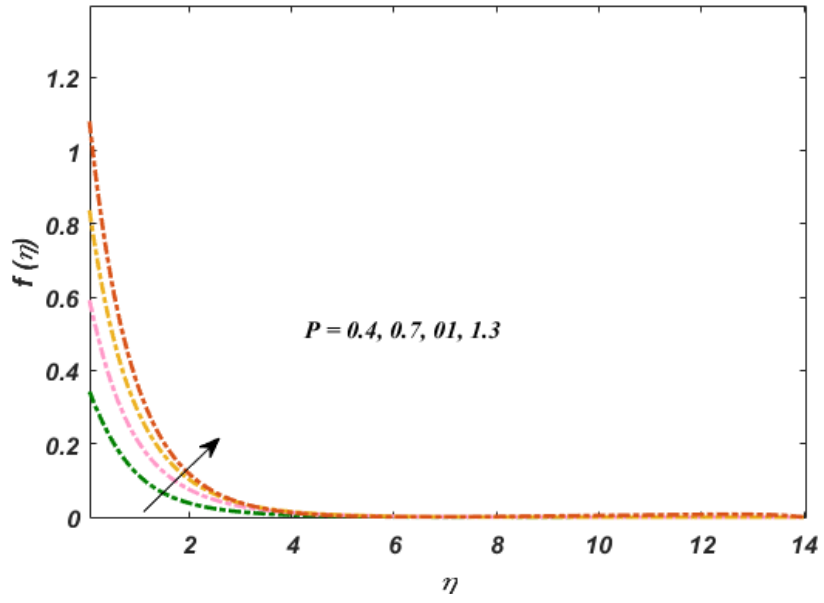Fig. 4.14 change in $g(\eta)$ vs.L
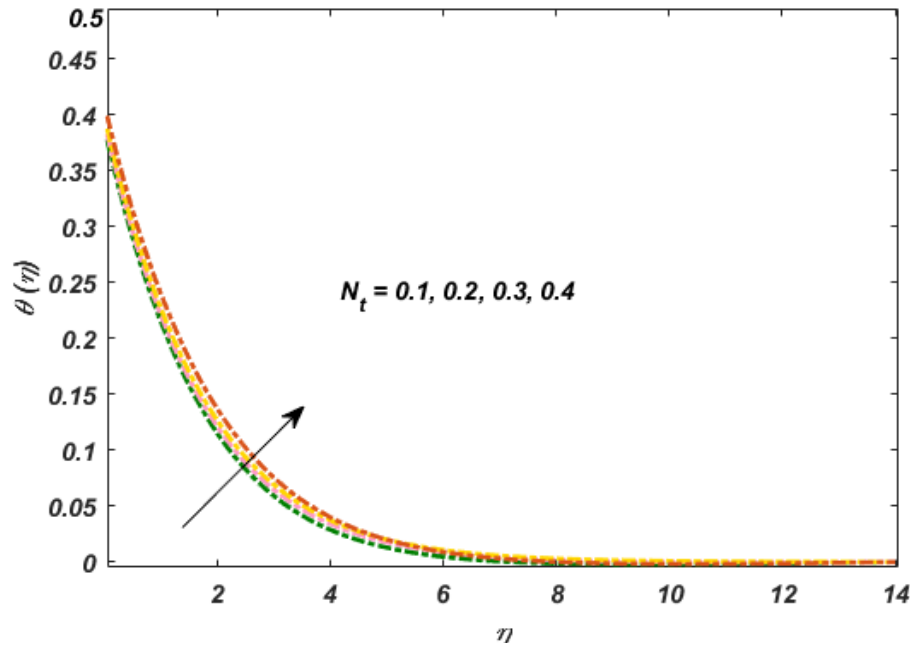
Fig. 4.15 change in $f(\eta)$ vs p

Fig. 4.16 change in $\theta(\eta)$ vs N_t

Fig. 4.17 change in $\theta(\eta)$ vs $.N_b$

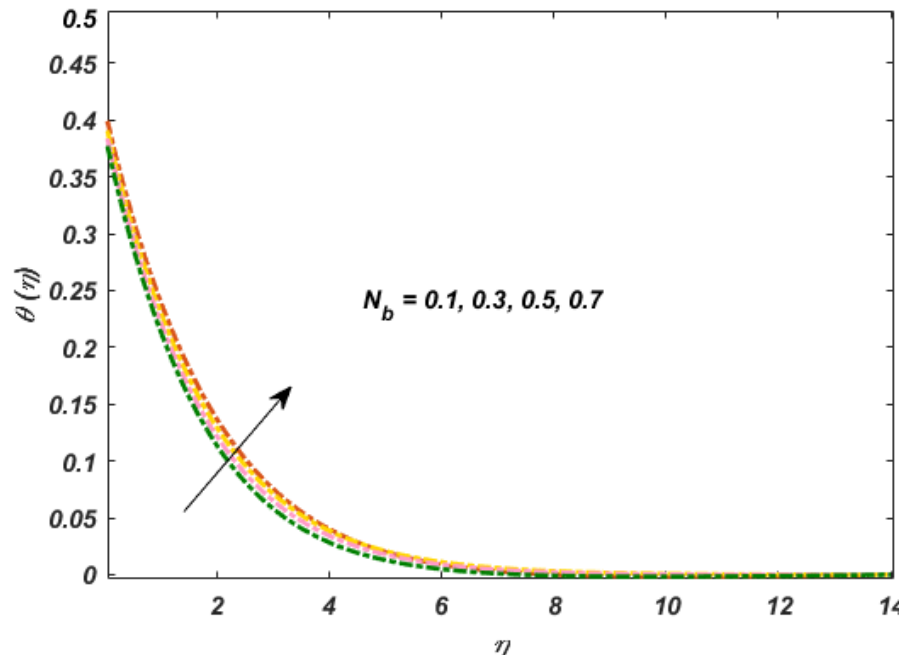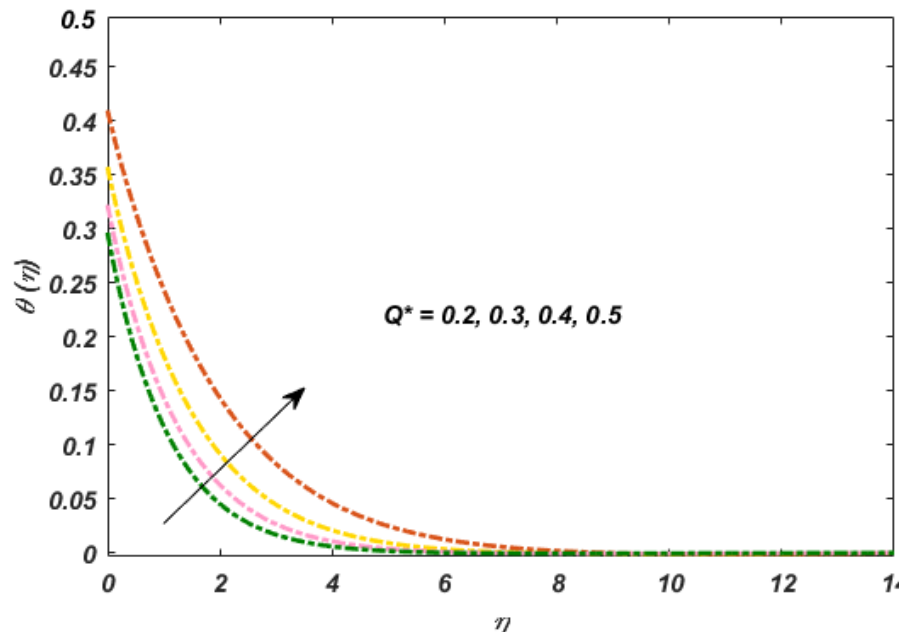Fig. 4.18 change in $\theta(\eta)$ vs Q^*

69
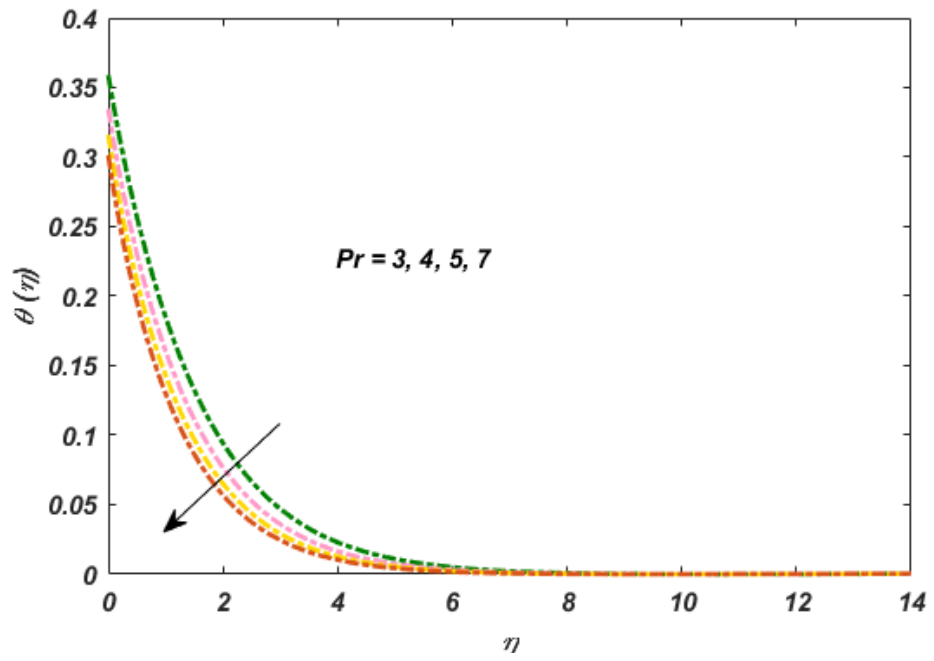
Fig. 4.19 change in $\theta(\eta)$ vs p_r
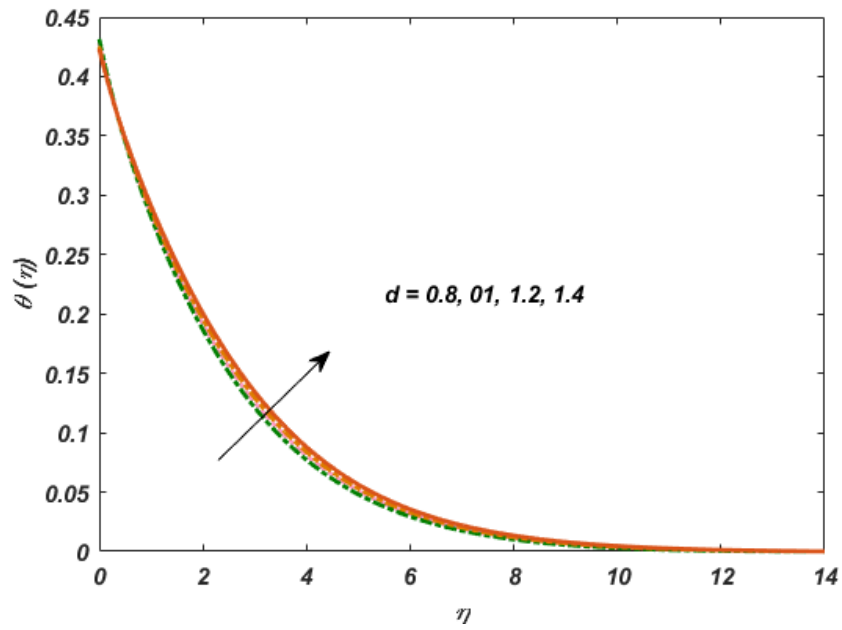
Fig. 4.20 change in $\theta(\eta)$ vs d
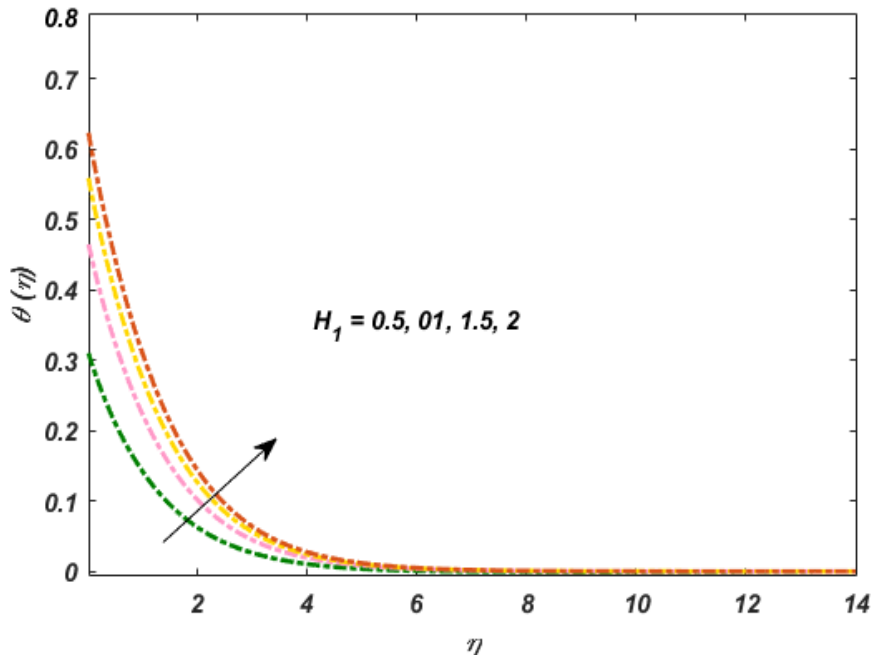
Fig. 4.21 change in $\theta(\eta)$ vs H_1
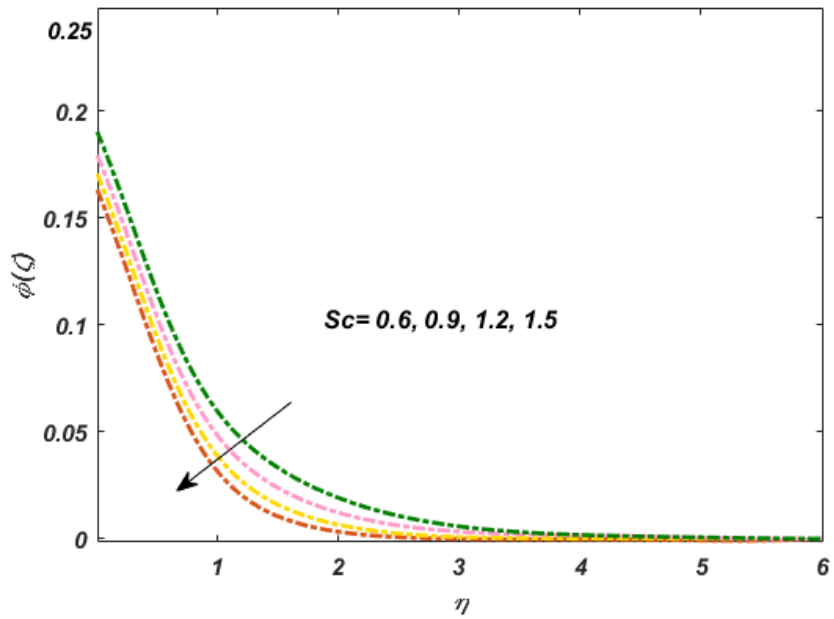
Fig. 4.22 change in $\phi(\eta)$ vs Sc
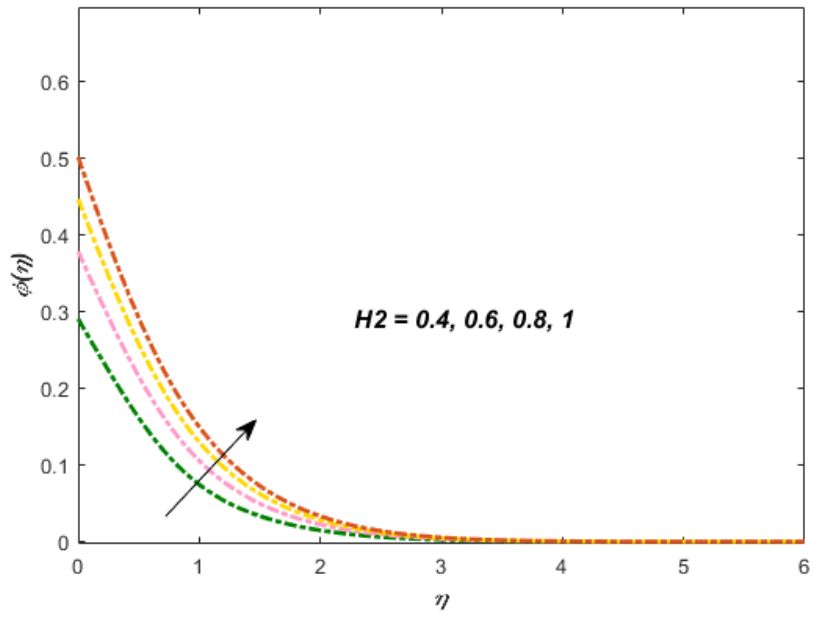
Fig. 4.23 change in $\phi(\eta)/\eta s.H_2$
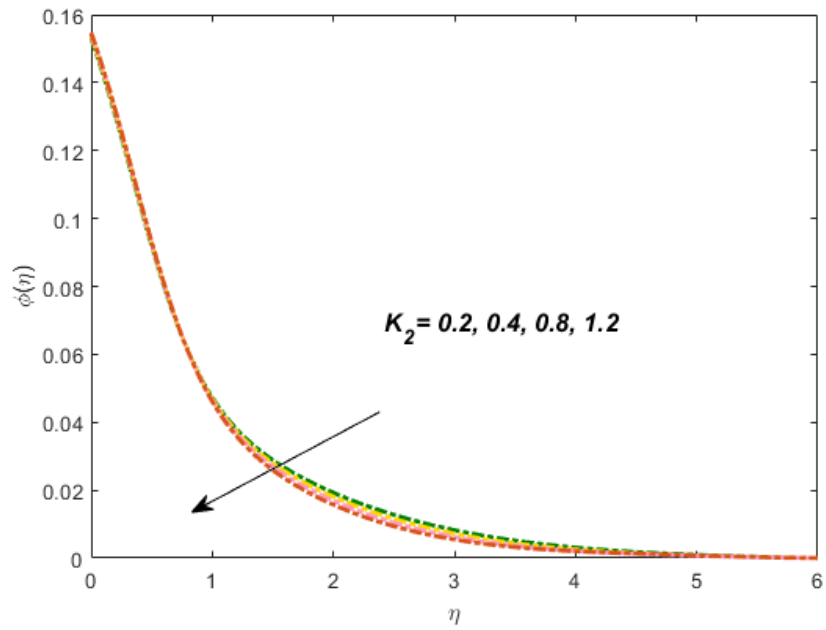
Fig. 4.24 change in $\phi(\eta)$ $vs.$ K_2
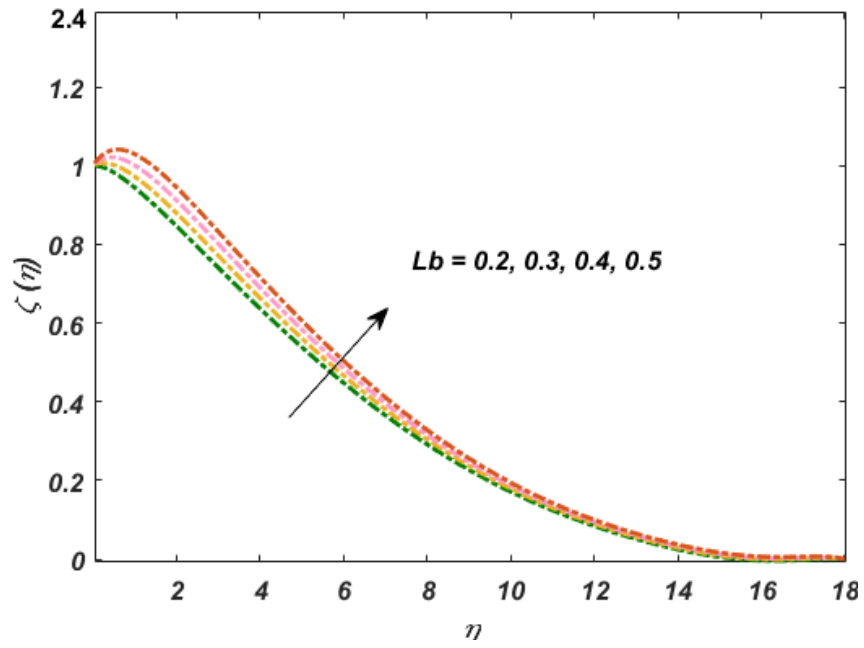
Fig. 4.25 change in $\zeta(\eta)/$ vs Lb
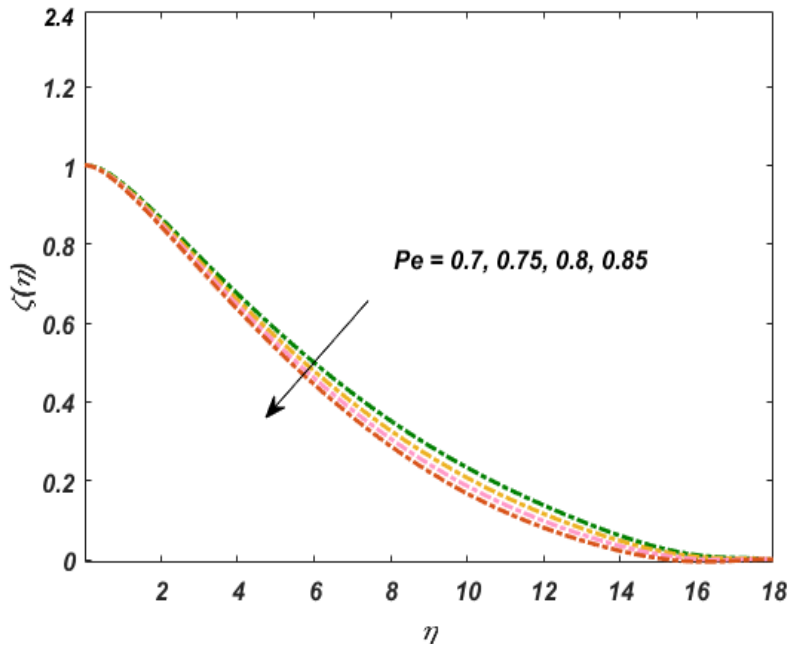
Fig. 4.26 change in $\zeta(\eta)$ vs. Pe

Table 4.1 : Computational values of friction drag coefficient $C_f \left(\text{Re}_r\right)^{0.5}$ for diffrent of β_1, λ^* and M.

β_1	λ^*	M	$C_f \left(\text{Re}_r\right)^{0.5}$
0.2		0.5	1.9114304
0.4			1.5667328
0.6			1.2715703
	0.4		1.3192113
	0.8		1.8198023
	1.2		1.9803022
		02	1.8235742
		2.5	1.6081978
		03	1.0548071

Table 4.2: Computational values of $Nu_r \, \mathrm{Re}_r^{-0.5}$, against different estimation Pr, N_t, Q^*, N_b, d, K_1 and $H_{1,}$.

Pr	N_t	Q^*	N_b	d	K_1	H_1	$Nu_r\sqrt{\mathrm{Re}_r}$
3	1.0	0.2	0.1	0.8	1	0.5	0.3366450
4							0.34866874
5							0.35768898
	0.2						0.36000232
	0.3						0.36199765
	0.4						0.36392501
		0.3					0.32195468
		0.4					0.34735602
		0.5					0.37395898
			0.3				0.37430140
			0.5				0.37302038
			0.7				0.37012750
				1			0.37094601
				1.2			0.36948448
				1.4			0.36780321
					2		0.36779493
					3		0.36778641
						1	0.61549357
						1.5	0.78419589
						2	0.91171466

Table 4.3: numerical values of for distint values of $Sc, H_2,\ K_2,$ and e .

S_c	e	K_2	H_2	$-Sh_r\sqrt{\mathrm{Re}_r}$
0.6	0.1	0.2	0.4	0.76722018
0.9				0.78364562
1.2				0.79214914
	0.2			0.79544019
	0.3			0.80136458
	0.4			0.80122596
		0.4		0.80966742
		0.6		0.8271761
		0.8		0.83318923
			0.6	0.9345602
			0.8	0.98525127
			01	1.0197144

Table 4.4: Validation of $f(0), -j(0)$ and - $\theta(0)$ when $\lambda^* = M = \beta_i = \beta_e = 0$, $\beta_1 \rightarrow \infty, Nb \rightarrow 0$, $Pr = 6$, with Shaheen et al [59], Hafeez et al.[58], Yin et al. [57] and Turkyilmazoglu [56] with the present work

	Shaheen, et al. [59]	Hafeez et al. [58]	Yin et al. [57]	Turkyilmazoglu [56]	Present
$f(0)$	0.51026466	0.51011626	0.51022941	0.51023262	0.510217375
$-g'(0)$	0.61594897	0.61584927	0.61591990	0.61592201	0.615810375
$-\theta'(0)$	0.93386285	0.933697411	0.93387285	0.93387794	0.933729175

Chapter 5

CONCLUSIONS AND FUTURE WORK

We studied two problems in this thesis. First one is review work whille other is extended work. Conclusions for both problems are as follows.

5.1 Chapter 3

In this study,we have analzed the Casson nanofluid flow over a rotating deformable disk in a Darcy–Forchhemier permeable medium under the impact of variable thermal conductivity and variable thermal diffusivity. The effects of the Hall current, Fick and Fourier laws, and heat absorption\generation with slip and convective boundary conditions are also considered. The mathematical model is Numerically solved technique using bvp4c.The noteworthy observations of the model are appended as below:

- The fluid velocity is diminished for the higher Casson parameter.

- For different values of Hall current parameter, velocity profile increases in the radial direction and an opposing trend is seen for the azimuthal direction.

- The concentration field augments for growing estimates of the activation energy. Similarly, the rate of mass transfer escalates on varying the chemical reaction parameter.

- For larger values of thermal and concentration relaxation parameter, the fluid temperatures and concentration fields decrease.

- For increasing values of the variable molecular diffusivity parameter, the rates of concentration decreases.

5.2 Chapter 4

In the present consieration, we have investigated the Maxwell nanofluid flow over a rotating deformable disk under the impact of magnetic field, variable viscosity, thermal conductivity, thermal diffusivity and gyrotactic microorganisms. The effect of Hall current and Ion-slip, and heat absorption\generation with slip and convective boundary conditions are also considered. The mathematical model is Numerically using bvp4c, a MATLAB-implemented function.The noteworthy observations of the model are appended as below:

- For different values of Hall current parameter velocity profile increares in the radial direction while opposite trend is seen in the azimuthal direction.

- For different values of Ion-sip parameter, velocity profile increases in the radial direction while decreasing in the azimuthal direction.

- Higher estimations of the thermal relaxation parameter and concentration relaxation parameter, the temperature and concentration profiles are decreasing.

- For higher estimations of the variable molecular diffusivity parameter, the rates of concentration decreases.

- The concentration profile is reduced for varied values of the Schmidt number.

- Higher estimations of the Bioconvective peclet number (Pe) and concentration difference parameter (Ω) the motile density profile is decreased.

5.3 Future work

The interesting possible extensions that could be researched in future are ae follows;

- The fluid flow may be exttended to the any other non-newtonian fluid.

- Boundary conditions also be changed to melting heat or second order slip.

Bibliography

[1] Choi, S. U., & Eastman, J. A. Enhancing thermal conductivity of fluids with nanoparticles (No. ANL/MSD/CP-84938; CONF-951135-29),1995.

[2] Buongiorno, Jacopo. "Convective transport in nanofluids." (2006): 240-250.

[3] Feteca C, Vieru D, Azhar WA. Natural convection flow of fractional nanofluid sover an isothermal vertical plate with thermal radiation. Appl. Sci. ;(2017): 7:247,

[4] Bhatti, M. M., & Rashidi, M. M. Effects of thermo-diffusion and thermal radiation on Williamson nanofluid over a porous shrinking/stretching sheet. Journal of Molecular Liquids, 221, (2016): 567-573, .

[5] Turkyilmazoglu M. Flow of nanofluid plane wall jet and heat transfer. European Journal of Mechanics - B/Fluids ;59:(2021) 18–24.

[6] Venthan, S. M., Amalraj, I. J., & Kumar, P. S. Analysis of entrance region flow of Bingham nanofluid in concentric annuli with rotating inner cylinder. Micro & Nano Letters, 14(13), (2019): 1361-1365.

[7] Waqas, H., Imran, M., Khan, S. U., Shehzad, S. A., & Meraj, M. A. Slip flow of Maxwell viscoelasticity-based micropolar nanoparticles with porous medium: a numerical study. Applied Mathematics and Mechanics, 40(9),(2019): 1255-1268.

[8] Ali, M., Sultan, F., Khan, W. A., Shahzad, M., & Arif, H. Important features of expanding/contracting cylinder for Cross magneto-nanofluid flow. Chaos, Solitons & Fractals, 133, (2020): 109656.

[9] Ghalambaz M, Mehryan SAM, Hajjar A, Veismoradi A. Unsteady natural convection flow of a suspension comprising Nano-Encapsulated Phase Change Materials (NEPCMs) in a porous medium. Advanced Powder Technology, 31(3):(2020): 954–66.

[10] Rafiq, M., Shafique, M., Azam, A., & Ateeq, M. Transformer oil-based nanofluid: The application of nanomaterials on thermal, electrical and physicochemical properties of liquid insulation-A review. Ain Shams Engineering Journal, 12(1), (2021): 555-576.

[11] Javadzadegan, A., Motaharpour, S. H., Moshfegh, A., Akbari, O. A., Afrouzi, H. H., & Toghraie, D. Lattice-Boltzmann method for analysis of combined forced convection and radiation heat transfer in a channel with sinusoidal distribution on walls. Physica A: Statistical Mechanics and its Applications, 526,(2021): 121066.

[12] Alrashed, A. A., Akbari, O. A., Heydari, A., Toghraie, D., Zarringhalam, M., Shabani, G. A. S & Goodarzi, M. The numerical modeling of water/FMWCNT nanofluid flow and heat transfer in a backward-facing contracting channel. Physica B: Condensed Matter, 537, (2011):176-183,.

[13] Sharma, K., Vijay, N., Mabood, F., & Badruddin, I. A. Numerical simulation of heat and mass transfer in magnetic nanofluid flow by a rotating disk with variable fluid properties. International Communications in Heat and Mass Transfer, 133,(2022): 105977.

[14] Alsallami, S. A., Zahir, H., Muhammad, T., Hayat, A. U., Khan, M. R., & Ali, A. . Numerical simulation of Marangoni Maxwell nanofluid flow with Arrhenius activation energy and entropy anatomization over a rotating disk. Waves in Random and Complex Media, (2021): 1-19.

[15] Naveed Khan, M., Ahmad, S., Ahammad, N. A., Alqahtani, T., & Algarni, S. Numerical investigation of hybrid nanofluid with gyrotactic microorganism and multiple slip conditions through a porous rotating disk. Waves in Random and Complex Media, (2021): 1-16.

[16] Von Karman, T. Uberlaminare und turbulente reibung, Zeit. Angew. Math. Mech, 1. (1921).

[17] Turkyilmazoglu, M. Effects of uniform radial electric field on the MHD heat and fluid flow due to a rotating disk. International Journal of Engineering Science, 51, (2012): 233-240.

[18] Khan, N., Hashmi, M. S., Khan, S. U., & Syed, W. A. Study of polymeric liquid between stretching disks with chemical reaction. Journal of the Brazilian Society of Mechanical Sciences and Engineering, 40(2), (2012): 1-15.

[19] Von Kármán, T. Uber laminare und turbulente Reibung. Journal of Applied Mathematics and Mechanics / Zeitschrift für Angewandte Mathematik, 1,(1921): 233-252.

[20] Cochran, W. G. The flow due to a rotating disc. In Mathematical proceedings of the Cambridge philosophical society (Vol. 30, No. 3,1934 July: 365-375).

[21] Benton, E. R. On the flow due to a rotating disk. Journal of Fluid Mechanics, 24(4),(1966): 781-800.

[22] Hafeez, A., Khan, M., & Ahmed, J. Oldroyd-B fluid flow over a rotating disk subject to Soret–Dufour effects and thermophoresis particle deposition. Proceedings of the Institution of Mechanical Engineers, Part C: Journal of Mechanical Engineering Science, 235(13),(2021): 2408-2415.

[23] Ahmed, J., Khan, M., & Ahmad, L.Transient thin film flow of nonlinear radiative Maxwell nanofluid over a rotating disk. Physics Letters A, 383(12), (2019): 1300-1305.

[24] Mustafa, M., & Khan, J. A. Numerical study of partial slip effects on MHD flow of nanofluids near a convectively heated stretchable rotating disk. Journal of Molecular Liquids, 234, (2017): 287-295.

[25] Ijaz, M., & Ayub, M. Nonlinear convective stratified flow of Maxwell nanofluid with activation energy. Heliyon, 5(1),(2021): e01121,.

[26] Khan, Umair, Sardar Bilal, A. Zaib, O. D. Makinde, and Abderrahim Wakif. "Numerical simulation of a nonlinear coupled differential system describing a convective flow of Casson gold–blood nanofluid through a stretched rotating rigid disk in the presence of Lorentz forces and nonlinear thermal radiation." Numerical Methods for Partial Differential Equations 38, no. 3 (2022): 308-328.

[27] Khan, N., Riaz, I., Hashmi, M. S., Musmar, S. A., Khan, S. U., Abdelmalek, Z., & Tlili, I. Aspects of chemical entropy generation in flow of Casson nanofluid between radiative stretching disks. Entropy, 22(5),(2022): 495.

[28] Jana, R. N., & Dutta, N. Hall effects on MHD flow induced by torsional oscillations of a disc in a rotating fluid. Journal of Mathematical and Physical Sciences, 12(3),(1978): 253-265.

[29] Datta, S. The effect of Hall current on the torsional oscillation of a disc in a conduction fluid subjected to a uniform axial magnetic field. Matematički Vesnik, (55),(1971): 135-138.

[30] Mittal, M. L., & Bhat, A. N. Heat transfer by a developing magnetohydrodynamic flow with Hall and ion slip currents. In 4th National Heat and Mass Transfer Conference (1978): 247-253.

[31] Abo-Eldahab, E. M. and Aziz, M. A. E., "Hall and Ion-Slip Effects on MHD Free Convective Heat Generating Flow Past a Semi-Infinite Vertical Flat Plate," Physica Scripta, 61,(2000) pp. 344-348.

[32] Attia, H. A., Transient Hartmann Flow with Heat Transfer Considering the Ion Slip. Physica Scripta,66,(2002): 470-475.

[33] . Attia, H. A., "Unsteady Von-Karman Magnetic Flow and Heat Transfer Considering the Ion Slip,"International Communications Heat and Mass Transfer, 30,(2003): 535-543.

[34] Attia, H. A., Ion Slip Effect on the Flow Due to a Rotating Disk. The Arabian Journal of Science Engineering, 29,(2004): 165-172.

[35] Guria, M., A. K. Kanch, S. Das, and R. N. Jana. Effects of Hall current and slip condition on unsteady flow of a viscous fluid due to non-coaxial rotation of a porous disk and a fluid at infinity. Meccanica 45, no. 1 (2010): 23-32.

[36] Ghara, N., Das, S., Maji, S. L., & Jana, R. N. Effects of Hall Current and Ion-Slip on MHD Flow Induced by Torsional Oscillations of a Disc in a Rotating Fluid. Journal of Mechanics, 29(2),(2013): 337-344.

[37] Rafiq, T., Mustafa, M., & Farooq, M. A. Modeling heat transfer in fluid flow near a decelerating rotating disk with variable fluid properties. International Communications in Heat and Mass Transfer, 116,(2022): 104673.

[38] Khan, M., Salahuddin, T., & Stephen, S. O. Thermo-physical characteristics of liquids and gases near a rotating disk. Chaos, Solitons & Fractals, 141,(2022): 110304.

[39] Ahmed, J., Khan, M., & Ahmad, L. Stagnation point flow of Maxwell nanofluid over a permeable rotating disk with heat source/sink. Journal of Molecular Liquids, 287,(2022): 110853.

[40] Hayat, T., Javed, M., Imtiaz, M., & Alsaedi, A. Effect of Cattaneo-Christov heat flux on Jeffrey fluid flow with variable thermal conductivity. Results in physics, 8,(2022): 341-351.

[41] Abbas, W., Mekheimer, K. S., Ghazy, M. M., & Moawad, A. M. A. Thermal radiation effects on oscillatory squeeze flow with a particle-fluid suspension. Heat Transfer, 50(3), (2021): 2129-2149.

[42] Abdelmalek, Z., Khan, S. U., Waqas, H., Al-Khaled, K., & Tlili, I. A proposed unsteady bioconvection model for transient thin film flow of rate-type nanoparticles configured by rotating disk. Journal of Thermal Analysis and Calorimetry, 144(5), (2021): 1639-1654.

[43] Kuznetsov, A. V. Nanofluid bioconvection in water-based suspensions containing nanoparticles and oxytactic microorganisms: oscillatory instability. Nanoscale research letters, 6(1),(2021): 1-13.

[44] Raju, C. S. K., Hoque, M. M., & Sivasankar, T. Radiative flow of Casson fluid over a moving wedge filled with gyrotactic microorganisms. Advanced Powder Technology, 28(2), (2017): 575-583.

[45] Alsaedi, A., Khan, M. I., Farooq, M., Gull, N., & Hayat, T. Magnetohydrodynamic (MHD) stratified bioconvective flow of nanofluid due to gyrotactic microorganisms. Advanced Powder Technology, 28(1),(2017): 288-298.

[46] Alsaedi, A., Khan, M. I., Farooq, M., Gull, N., & Hayat, T. Magnetohydrodynamic (MHD) stratified bioconvective flow of nanofluid due to gyrotactic microorganisms. Advanced Powder Technology, 28(1),(2017): 288-298.

[47] Khan, W. A., Rashad, A. M., Abdou, M. M. M., & Tlili, I. Natural bioconvection flow of a nanofluid containing gyrotactic microorganisms about a truncated cone. European Journal of Mechanics-B/Fluids, 75, (2019): 133-142.

[48] Waqas, H., Khan, S. U., Hassan, M., Bhatti, M. M., & Imran, M. Analysis on the bioconvection flow of modified second-grade nanofluid containing gyrotactic microorganisms and nanoparticles. Journal of Molecular Liquids, 291, (2019): 111231.

[49] Alwatban, A. M., Khan, S. U., Waqas, H., & Tlili, I. Interaction of Wu's slip features in bioconvection of Eyring Powell nanoparticles with activation energy. Processes, 7(11),(2019): 859.

[50] Rafiq, T., Mustafa, M., & Farooq, M. A. Modeling heat transfer in fluid flow near a decelerating rotating disk with variable fluid properties. International Communications in Heat and Mass Transfer, 116,(2019): 104673.

[51] Ahmed, J., Khan, M., Ahmad, L., Alzahrani, A. K., & Alghamdi, M. Thermally radiative flow of Maxwell nanofluid over a permeable rotating disk. Physica Scripta, 94(12),(2019): 125016.

[52] Qasim, M., Afridi, M. I., Wakif, A., & Saleem, S. . Influence of variable transport properties on nonlinear radioactive Jeffrey fluid flow over a disk: utilization of generalized differential quadrature method. Arabian Journal for Science and Engineering, 44(6), (2020): 5987-5996.

[53] Naganthran, K., Mustafa, M., Mushtaq, A., & Nazar, R. Dual solutions for fluid flow over a stretching/shrinking rotating disk subject to variable fluid properties. Physica A: Statistical Mechanics and Its Applications, 556, (2020):124773.

[54] Khan, M., Salahuddin, T., & Stephen, S. O. Variable thermal conductivity and diffusivity of liquids and gases near a rotating disk with temperature dependent viscosity. Journal of Molecular Liquids, 333, (2021):115749.

[55] Ahmed, J., Khan, M., & Ahmad, L. Effectiveness of homogeneous–heterogeneous reactions in Maxwell fluid flow between two spiraling disks with improved heat conduction features. Journal of Thermal Analysis and Calorimetry, 139(5), (2020): 3185-3195.

[56] Turkyilmazoglu, M. Nanofluid flow and heat transfer due to a rotating disk. Computers & Fluids, 94,(2014): 139-146.

[57] Yin, C., Zheng, L., Zhang, C., & Zhang, X. Flow and heat transfer of nanofluids over a rotating disk with uniform stretching rate in the radial direction. Propulsion and Power Research, 6(1), (2017): 25-30

[58] Hafeez, A., Khan, M., & Ahmed, J. Flow of Oldroyd-B fluid over a rotating disk with Cattaneo–Christov theory for heat and mass fluxes. Computer methods and programs in biomedicine, 191,(2020): 105374.

[59] Shaheen, N., Ramzan, M., & Alaoui, M. K. Impact of Hall current on a 3D Casson nanofluid flow past a rotating deformable disk with variable characteristics. Arabian Journal for Science and Engineering, 46(12), (2022): 12653-12666.

[60] Ramzan, M., Gul, H., Mursaleen, M., Nisar, K. S., Jamshed, W., & Muhammad, T. Von Karman rotating nanofluid flow with modified Fourier law and variable characteristics in liquid and gas scenarios. Scientific Reports, 11(1), (2021): 1-17.

Jawad 456

18%	8%	15%	4%
SIMILARITY INDEX	INTERNET SOURCES	PUBLICATIONS	STUDENT PAPERS

PRIMARY SOURCES

1	link.springer.com Internet Source	1%
2	Submitted to Higher Education Commission Pakistan Student Paper	1%
3	Muhammad Ramzan, Jae Dong Chung, Naeem Ullah. "Radiative magnetohydrodynamic nanofluid flow due to gyrotactic microorganisms with chemical reaction and non-linear thermal radiation", International Journal of Mechanical Sciences, 2017 Publication	1%
4	Naila Shaheen, Muhammad Ramzan, M. Kbiri Alaoui. "Impact of Hall Current on a 3D Casson Nanofluid Flow Past a Rotating Deformable Disk with Variable Characteristics", Arabian Journal for Science and Engineering, 2021 Publication	1%